Far Infrared Spectroscopy of Normal Galaxies: Physical Conditions in the Interstellar Medium

S. Malhotra [1,2], M. J. Kaufman[3,4], D. Hollenbach[4], G. Helou[5], R. H. Rubin[4], J. Brauher[5], D. Dale[5], N. Y. Lu[5], S. Lord[5], G. Stacey[6], A. Contursi[5], D. A. Hunter[7], H. Dinerstein[8]

ABSTRACT

The most important cooling lines of the neutral interstellar medium (ISM) lie in the far-infrared (FIR). We present measurements by the Infrared Space Observatory Long Wavelength Spectrometer of seven lines from neutral and ionized ISM of 60 normal, star-forming galaxies. The galaxy sample spans a range in properties such as morphology, FIR colors (indicating dust temperature), and FIR/Blue ratios (indicating star-formation activity and optical depth).

In two-thirds of the galaxies in this sample, the [C II] line flux is proportional to FIR dust continuum. The other one-third show a smooth decline in $L_{[CII]}/L_{FIR}$ with increasing $F_\nu(60\ \mu m)/F_\nu(100\ \mu m)$ and L_{FIR}/L_B, spanning a range of a factor of more than 50. Two galaxies, at the warm and active extreme of the range have $L_{[CII]}/L_{FIR} < 2 \times 10^{-4}(3\sigma$ upper limit). This is due to increased positive grain charge in the warmer and more active galaxies, which leads to less efficient heating by photoelectrons from dust grains.

The ratio of the two principal photodissociation region (PDR) cooling lines $L_{[OI]}/L_{[CII]}$ shows a tight correlation with $F_\nu(60\ \mu m)/F_\nu(100\ \mu m)$, indicating that both gas and dust temperatures increase together. We derive a theoretical scaling between [N II](122 μm) and [C II] from ionized gas and use it to separate [C II] emission from neutral PDRs and ionized gas. Comparison of PDR models of Kaufman et al. (1999) with observed ratios of (a) $L_{[OI]}/L_{[CII]}$ and $(L_{[CII]} + L_{[OI]})/L_{FIR}$ and (b) $L_{[OI]}/L_{FIR}$ and $F_\nu(60\ \mu m)/F_\nu(100\ \mu m)$ yields far-UV flux G_0 and gas density n. The G_0 and n values estimated from the two methods agree to better than a factor of 2 and 1.5 respectively in more than half the sources.

The derived G_0 and n correlate with each other, and G_0 increases with n as $G_0 \propto n^\alpha$, where $\alpha \approx 1.4$. We interpret this correlation as arising from Strömgren sphere scalings if much of the line and continuum luminosity arises near star-forming regions. The high values of PDR surface temperature $(270 - 900\,K)$ and pressure $(6 \times 10^4 - 1.5 \times 10^7\,K\,cm^{-3})$ derived also support the view that a significant part of grain and gas heating in the galaxies occurs very

close to star-forming regions. The differences in G_0 and n from galaxy to galaxy may be due to differences in the physical properties of the star-forming clouds. Galaxies with higher G_0 and n have larger and/or denser star-forming clouds.

Subject headings: radiation mechanisms: thermal, ISM: atoms, ISM: general, ISM: H II regions, galaxies: ISM, infrared: ISM: lines and bands

1. Introduction

The atomic and ionic fine-structure lines [C II] (158 μm) and [O I] (63μm) are the dominant cooling lines for neutral interstellar gas, and ionic fine-structure lines like [O III] (88 μm), (52 μm) and [N II] (122 μm) are strong coolants in H II regions. These lines can be used as diagnostics to infer physical conditions in the gas, such as temperatures, densities and radiation fields, by comparing with models of photodissociation regions (PDRs e.g. Tielens & Hollenbach 1985, Sternberg & Dalgarno 1989, Wolfire, Tielens & Hollenbach 1990, Kaufman et al. 1999) and H II regions (Rubin et al. 1991).

Among these, [C II] is the most ubiquitous and best studied line. It was predicted to be the dominant coolant for diffuse neutral media by Dalgarno & McCray (1972), but the first detection of this line was towards the dense star-forming regions M42 and NGC 2024 (Russell et al. 1980). The early observations of external galaxies were of nearby or IR bright galaxies and showed that [C II] emission was associated with dense gas irradiated by ultra-violet (UV) light from young star-forming regions, often near galactic nuclei (Crawford et al. 1985, Stacey et al. 1991). Later, observations of quiescent galaxies like NGC 6946 showed that averaged over the whole disk, including the HI-rich outer disk, a significant fraction of the total [C II] in a galaxy may arise from diffuse ionized or diffuse atomic gas

[1]Johns Hopkins University, Charles and 34th Street, Bloomberg Center, Baltimore, MD 21210

[2]Hubble Fellow

[3]Dept. of Physics, San José State University, One Washington Square, San José, CA 95192-0106

[4]NASA/Ames Research Center, MS 245-3, Moffett Field, CA 94035

[5]IPAC, 100-22, California Institute of Technology, Pasadena, CA 91125

[6]Cornell University, Astronomy Department, 220 Space Science Building, Ithaca, NY 14853

[7]Lowell Observatory, 1400 Mars Hill Rd., Flagstaff, AZ 86001

[8]University of Texas, Astronomy Department, RLM 15.308, Texas Austin, TX 78712

(Madden et al. 1993, but see Contursi et al. 2001). Observations of many FIR lines in the Milky Way by FIRAS , including [C II] (158 μm) and [N II] (205 μm), indicated that a fair, and possibly dominant, fraction of [C II] emission is from diffuse ($n_e = 1 - 5$ cm^{-3}) ionized gas (Petuchowski & Bennett 1993, Heiles 1994). Recent ISO observations have yielded more surprises. In a previous paper we reported a deficiency of [C II] compared with FIR continuum in three normal star-forming galaxies (Malhotra et al. 1997, Paper I). A similar deficiency was reported for ultraluminous galaxies by Luhman et al. (1998).

The range of interpretations for the origin and behavior of the [C II] line in particular, and FIR cooling lines in general, emphasizes the need for studying a suite of FIR lines in a large sample of galaxies. The Long Wavelength Spectrometer (LWS, Clegg et al. 1996) on the Infrared Space Observatory (ISO, Kessler et al. 1996) has made it possible to observe a large number of atomic and ionic fine-structure lines in the FIR with unprecedented sensitivity, so that a large sample of galaxies could be observed.

In this paper we report on and interpret observations of fine structure atomic and ionic lines observed in 60 normal galaxies. The sample consists of galaxies whose luminosity is dominated by star-formation and excludes Active Galactic Nuclei (AGN). We observed 60 distant galaxies, for which all the FIR emission is within one LWS beam, as well as 6 nearby, resolved galaxies. Here we report on the distant sample.

We observed from one to seven atomic and ionic fine structure lines for each galaxy depending on its FIR brightness. The lines include [C II](158μm), [O I](145μm), [N II](122μm), [O III] (88μm), [O I](63μm), N III (57μm) and [O III] (52μm). The most common lines observed are [C II](158μm), [O I](63μm), [O III] (88μm) and [N II](122μm). There is no convincing detection of N III (57μm), so we do not discuss that line here. This paper offers a look at the statistical behavior of [C II], [N II], [O III] and [O I] lines in a diverse sample of galaxies, aimed at better understanding the physical conditions in the Interstellar medium (ISM) of normal star-forming galaxies.

The paper is arranged as follows: in Section 2, we discuss the far-infrared lines observed, their properties, and their diagnostic value in deriving the physical conditions in the ISM. In Section 3 we discuss the observations and data reduction procedures. In Section 4 we describe the statistical trends observed; in Section 5 we interpret these trends, and in Section 6 we discuss the physical conditions in the PDRs in these galaxies. Section 7 contains conclusions and a summary of the main results. Appendix A contains a description of the sample selection and how the sample spans the parameter space in galaxy properties. Appendices B and C contain tables of line fluxes and derived physical quantities: far-UV flux G_0, gas density n, temperature T and pressure P.

2. Far Infrared Fine structure lines

Table 1: Properties of FIR lines observed

Species	Wavelength (μm)	Excitation Potential [a](eV)	Ionization Potential [b](eV)	$T = \Delta E/k$ (Kelvin)	n_{crit} [c] cm^{-3}
[C II]	157.714	11.26	24.38	91	3×10^3 [H]
					5×10^3 [H_2], 50[e][1]
[O I]	145.525	-	13.62	98	$1 \times 10^5 (T/100)^{-0.57}$ [H]
					$8 \times 10^4 (T/100)^{-0.34}$ [H_2]
[O I]	63.183			228	$8.5 \times 10^5 (T/100)^{-0.69}$ [H] [2,3]
					$4 \times 10^5 (T/100)^{-0.34}$ [H_2] [4]
[N II]	121.89	14.53	29.6		3.1×10^2 [e] [1]
[O III]	88.356	35.12	54.93		5.1×10^2 [e] [1]
	51.815				3.6×10^3 [e] [1]
N III	57.317	29.60	47.45		3×10^3 [e] [1]

[a] Potential required to create the ion

[b] Potential required to ionize the species

[c] critical density

[1] Genzel 1991

[2] Hollenbach & McKee 1989

[3] Launay & Roeff 1977

[4] Jaquet et al. 1992

Table 1 summarizes the properties of the lines observed for this sample and discussed in this paper (cf. Genzel 1991 for a more exhaustive description of atomic, ionic and molecular lines in the infrared). Here critical density for a transition is the density at which collisions balance spontaneous radiative transitions. $T = \Delta E/k$ indicates the temperature corresponding to the energy difference in the upper and lower levels.

2.1. [C II]

The C^+ fine structure transition at 157.714 μm is the most important coolant of the warm neutral interstellar medium. Carbon is the fourth most abundant element and has a lower ionization potential (11.26 eV) than hydrogen, so that carbon will be in the form of C^+ in the neutral surface layers of far-UV illuminated neutral gas clouds. The depth of

these C^+ zones is generally determined by dust extinction and often extends to $A_V \leq 4$. The 158 μm [C II] line is also relatively easy to excite (ΔE/k $\simeq$ 91 K), so that C^+ can cool warm ($30\,K < T < 10^4$ K) neutral gas where the two most abundant atoms H and He cannot (cf. Tielens & Hollenbach (1985), hereafter TH85; Wolfire, Tielens & Hollenbach 1990, hereafter WTH90). In the C^+ zones of PDRs, the electrons are supplied by the C^+ ions so that the abundance of electrons relative to hydrogen is $x(e) \simeq 10^{-4}$. In such conditions the [C II](158 μm) line is excited by collisions with hydrogen atoms

[C II] from neutral regions can be used in combination with the [O I] lines and the FIR continuum, to derive the gas density n and the incident FUV (6 eV $<$ hν $<$ 13.6 eV) radiation flux G_0 respectively (e.g. Wolfire, Tielens & Hollenbach 1990; Kaufman et al. 1999). G_0 conventionally is the FUV flux normalized to the average local interstellar flux of 1.6×10^{-3} ergs cm^{-2} s^{-1} (Habing 1968). Since [C II] comes from both ionized and neutral regions, decomposing the two components may be necessary before the comparison with [O I] can be made.

2.2. [N II]

Since nitrogen has an ionization potential (14.5 eV) higher than that of hydrogen, [N II] (122 μm) arises only in ionized gas. This fine structure line is excited by collisions with electrons. [N II] (122 μm) has a critical electron density of $3.1 \times 10^2\,$cm^{-3}, and [C II] (158μm) has a critical electron density of 50 cm^{-3} (Table 1). We can estimate the [C II] arising from low density ($n_e < 50\,$cm^{-3}) ionized regions by comparison with the [N II] (122 μm) line, as described in section 5.4 below.

2.3. [O I]

Oxygen has an ionization potential of 13.62 eV, quite close to that of hydrogen, so atomic O is found in neutral regions only. In PDRs OI can exist in atomic form far deeper into clouds than C^+. All oxygen not incorporated into CO can stay atomic to depths as large as $A_V = 10$ if relatively high FUV fluxes impinge on a cloud (TH85). OI has two fine structure transitions, at 63μm and 145μm. The excitation energy of [O I](63 μm) corresponds to 228 K and the critical density is $\simeq 5 \times 10^5$cm^{-3} (at T $\simeq$ 300 K), so OI lines arise in warm and dense neutral regions. As discussed above, [O I](63 μm), [C II](158 μm) and the FIR continuum constrain G_0 and n. The 145μm line lies $\Delta E/k = 325$ K above the ground state so the ratio of [O I](145μm)/[O I] (63 μm) measures temperature

(or G_0) in the temperature range of $\simeq 300K$. In many cases, however, this ratio may be an indicator of optical depth in the 63μm line, which is often moderately optically thick. Early observations and modeling of the [O I] lines from Orion indicated that the 63 μm line was optically thick in emission from the Orion PDR (Stacey et al. 1983, 1993), while more recent observations of Sgr B2, DR21 and NGC6334 indicate self absorption in the [O I] line by intervening cool O along the line of sight (Keene et al. 1999; Poglitsch et al 1996; Kraemer et al. 1996).

2.4. [O III]

Since O II has an ionization potential of about 35 eV (Table 1), O III lines come from ionized regions of galaxies where the UV radiation field is dominated by fairly early type (≈O6) stars. The ratio of the two lines of [O III] at 88 μm and 52 μm is useful for determining electron density in H II regions. The n_e derived is insensitive to the temperature of electrons T_e (Rubin et al. 1994) and independent of abundance variations. Since the line ratios give a measure of local density, a large beam measurement by this technique gives $< n_e >$, as opposed to $< n_e^2 >^{1/2}$ provided by emission measures and observed extent.

2.5. N III

The ratio N III(57μm)/[N II](122 μm) provides a measure of the effective temperature of the ionizing star(s), T_{eff} (Rubin et al. 1994). N III(57μm) is only marginally detected in some sources and we are not sufficiently confident of the measured fluxes to include N III in this paper.

3. Observations and data analysis

All the line observations for this project were obtained using the low-resolution grating mode of LWS (Clegg et al. 1996). With the LWS spectral resolution of 0.29 and 0.6μm (for wavelength ranges 43-90.5 μm and 90.5-197 μm, respectively) we do not resolve the lines. Sixty distant galaxies were selected to have $FWHM < 30''$ in FIR emission using deconvolved IRAS maps . Therefore, with the LWS $70''$ beam, we report the total line fluxes for these galaxies, and, using measured distances, the total luminosities from these

galaxies [9]. The observations were made in LWS02 mode where the gratings are scanned across known lines. A few galaxies were observed in the LW01 mode where a complete scan was made to cover the wavelength range 45-193 μm.

The line observations were planned to achieve a sensitivity of a fixed fraction of the FIR continuum flux, depending on the expected line strength and the feasibility of the observations. Between one and seven of the lines [C II](158 μm), [O I](145 μm), [N II](122 μm), [O III] (88 μm), [O I](63 μm), N III (57 μm) and [O III] (52 μm) were observed for each of the 60 galaxies in the sample, depending on what was practical given the FIR brightness of the galaxy. The most commonly observed lines were [C II](158μm), [O I](63μm), [O III] (88μm) and [N II](122μm), in that order. Table 2 gives the planned sensitivities for the different lines along with the 1-σ noise actually achieved for these lines averaged over the whole sample of galaxies.

Table 2: Planned and achieved line sensitivities

Line	wavelength μm	1-σ flux (planned) (as a fraction of the continuum flux, F_{FIR})	Average 1-σ flux (achieved)
[C II]	158	2.2×10^{-4}	1.4×10^{-4}
[O I]	145	2.0×10^{-5}	3.0×10^{-5}
[N II]	122	8×10^{-5}	7.0×10^{-5}
[O III]	88	1×10^{-4}	1.3×10^{-4}
[O I]	63	1.0×10^{-4}	1.3×10^{-4}
N III	57	1.3×10^{-4}	2.1×10^{-4}
[O III]	52	2.4×10^{-4}	2.4×10^{-4}

The [C II] line observations were planned to achieve (1σ) sensitivities of $2.2\times10^{-4}\times F_{FIR}$, where F_{FIR} is the far-infrared flux of the galaxy between 42μm and 122μm and is computed according to the relation $F_{FIR} = 1.26 \times 10^{-14}[2.58 \times F_\nu(60\mu\text{m}) + F_\nu(100\mu\text{m})]Wm^{-2}$ (Helou et al. 1988), where $F_\nu(60\mu$m) and $F_\nu(100\mu$m) are flux densities in Jansky in the IRAS 60 and 100 μm bands. For comparison, previous observations of the Milky Way, starburst galaxies and galactic nuclei show that the line to continuum luminosity ratio $L_{[CII]}/L_{FIR} = 1 - 10 \times 10^{-3}$ (Stacey et al. 1985, Wright et al. 1991, Crawford et al. 1985, and Stacey et al. 1991). In Galactic PDRs associated with H II regions $L_{[CII]}/L_{FIR}$ varies from $\sim 3 \times 10^{-3}$ in NGC 2023 (a reflection nebula) to $\sim 8 \times 10^{-5}$ in W51, decreasing with H II region or PDR density and FUV flux (cf. Crawford et al. 1985, Hollenbach, Takahashi & Tielens 1991).

[9]In practice we will always use ratios, so the distance errors cancel

The data were calibrated with the ISO pipeline OLP7.0 and reduced by two methods. In the first method the line profiles were derived from several scans by running a median boxcar filter through them. An automatic rejection algorithm was used which discarded measurements more than 5σ away from the mean flux level and further discarded four measurements subsequent to the discarded points. This sigma-clipping gets rid of cosmic rays and a time-dependent rejection is done to remove possible memory effects on the detectors. The median of the observed fluxes is used instead of the mean to reduce the influence of outlying points arising from cosmic ray hits. The flux in the lines was determined by directly integrating under the line, after fitting a linear baseline to the underlying continuum measurements. The upper limits on non-detections were derived by calculating the flux from a hypothetical gaussian line with an amplitude of 3σ and the effective instrumental profile, since the lines are unresolved for all sources. In the second method, the individual scans were inspected and bad points were rejected after manual inspection. A linear baseline and a gaussian profile was then fit to the data. The line fluxes are derived from the fitted gaussian. The fluxes from the two methods agreed for well detected ($> 5\sigma$) sources. The line fluxes thus derived are tabulated in Appendix B.

Presently, the calibration uncertainties in the flux measurements are due to two sources: (1) ill-determined dark currents, which are additive in nature and affect the measured line fluxes minimally ($< 5\%$ in most cases) because the dark currents are subtracted with the continuum levels while determining the line flux; and (2) the absolute calibration and spectral response is tied to observations and a model atmosphere of Uranus. The relative flux calibration is determined by a measurement of a few bright lamps in between observations. We estimate that the flux uncertainty in our sources is better than 20%, including all random errors and systematic calibration terms. The instrument team reports calibration better that 10-15% for compact, bright sources observed on-axis (Swinyard et al. 1999).

4. Observations and Phenomenology

4.1. The [C II](158 μm) observations

While [C II] and [O I] are the main cooling lines of the neutral atomic ISM, the gas heating is dominated by photoelectrons from dust grains (Watson 1972; for a recent review see Hollenbach & Tielens 1999). In a fairly indirect and inefficient mechanism, incident FUV photons with energies high enough to eject electrons from dust grains (h $\nu > 6\ eV$) heat the gas via these photoelectrons, with a typical efficiency of $0.1 - 1\%$. Efficiency is defined as the energy input to the gas divided by the total energy of the FUV photons

absorbed by dust grains. This efficiency is determined by the microphysics of the grains, in particular the work function, photoelectric yield and the charge of the grains (which is determined by the ratio of FUV fluxes to gas density G_0/n). Before ISO observations little variation was seen in the total $L_{[CII]}/L_{FIR}$ of galaxies (Stacey et al. 1991, Crawford et al. 1985), or in the Milky Way at 7° scales (Wright et al. 1991). This suggested that averaged over galaxy scales, the heating efficiency did not vary much, and guided our line sensitivity choices, which were scaled to the FIR continuum.

The two circumstances where we do expect the [C II]/FIR ratio to change are: (1) for a high ratio of FUV flux to gas density, G_0/n, the grains get positively charged raising the potential barrier for photoelectric ejection, thereby dropping the heating efficiency; and (2) when the hardness of the radiation changes, changing the ratio of FUV light which is effective in photoelectric heating the gas to less energetic light which can only heat the dust. In subsequent sections we will see examples of each of these.

In a previous paper (Paper I) we presented [C II] measurements for half the current sample, and saw large variations in $L_{[CII]}/L_{FIR}$ including three non-detections of the [C II] line in sources with relatively large FIR continuum fluxes. With a full sample of 60 galaxies and with better calibrations we verify the main observational results of Paper I. From our comprehensive data (Table 6 and Figure 1) we observe:

(1) About two-thirds of the observed galaxies (41 out of 60) show a ratio $L_{[CII]}/L_{FIR} > 0.2\%$. This is consistent with models of photoelectric heating in PDRs illuminated by moderate FUV fluxes (TH85) and with previous observations (Stacey et al 1991).

(2) There is a trend of decreasing $L_{[CII]}/L_{FIR}$ with warmer FIR colors, $F_\nu(60\ \mu m)/F_\nu(100\ \mu m)$ and increasing star-formation activity, indicated by higher L_{FIR}/L_B ratios, where L_B is the luminosity in the B band. We test the significance of these correlations by performing the generalized Kendall's test (Isobe, Feigelson & Nelson 1986, Brown, Hollander & Korwar 1974) which accounts for censoring of data (i.e. upper limits). Since we don't know the exact functional form of the dependence of $L_{[CII]}/L_{FIR}$ on $F_\nu(60\ \mu m)/F_\nu(100\ \mu m)$ and L_{FIR}/L_B, a rank test is appropriate. That $L_{[CII]}/L_{FIR}$ and $F_\nu(60\ \mu m)/F_\nu(100\ \mu m)$ are uncorrelated is excluded at the 99.999% (4.4 σ) level. The anti-correlation between $L_{[CII]}/L_{FIR}$ and L_{FIR}/L_B is somewhat weaker and the hypothesis that $L_{[CII]}/L_{FIR}$ and L_{FIR}/L_B are uncorrelated is rejected at the 99.5% level (2.8σ).

(3) Three galaxies (NGC 4418, IC 0860 and CGCG 1510.8+0725) near the extreme end of this trend in the $F_\nu(60\ \mu m)/F_\nu(100\ \mu m)$ ratio and in the ratio of L_{FIR}/L_B showed no detectable line emission in the [C II] and [O I] lines, as reported in Paper I. Here we

report the observation of CGCG 1510.8+0725 with greater sensitivity and the detection of the [C II] line, consistent with the 3σ upper limit reported earlier. No other prominent lines, e.g. [O I] (63 μm), are seen in these galaxies.

Figure 1 also displays data from the sample of luminous and ultraluminous infrared galaxies (ULIRGs) of Luhman et al. (1998). They follow the same trends as normal galaxies.

We also explore the dependence of $L_{[CII]}/L_{FIR}$ on the total FIR luminosity of the galaxies (Figure 2). To extend the range of luminosity explored, we plot the normal galaxies as well as the ULIRGs from the sample of Luhman et al. (1998). There seems to be a dependence on the FIR luminosity, but many of the [C II] deficient galaxies lie in the middle of the luminosity range and the spread in $L_{[CII]}/L_{FIR}$ is large at the high luminosity end. With only the sample of normal galaxies the correlation between $L_{[CII]}/L_{FIR}$ and luminosity is significant at the 2.1σ level; adding the luminous and ultraluminous galaxies from the sample of Luhman et al. makes the correlation stronger (3.8 σ). We suspect that the dependence on luminosity is a secondary correlation and is due to the correlation between FIR colors and luminosity (Figure 13b in Appendix A).

4.2. The [N II] (122 μm) observations

[N II] at 122 μm arises from ionized gas, both in dense H II regions and diffuse ionized gas. Figure 3a shows the decrease of $L_{[NII]}/L_{FIR}$ with increasingly warm FIR colors. Unfortunately the detections are fewer than for the [C II] (158 μm) and [O I](63μm) lines. We detected this line in about 36% (19 of 52) of the galaxies observed, and the entire range of $L_{[NII]}/L_{FIR}$, including upper limits, is only about a factor of 12. Figure 3a suggests that [NII] follows similar trends as [C II]; i.e. $L_{[NII]}/L_{FIR}$ decreases with $F_\nu(60\ \mu m)/F_\nu(100\ \mu m)$. The anticorrelation between $L_{[NII]}/L_{FIR}$ and $F_\nu(60\ \mu m)/F_\nu(100\ \mu m)$ is 2.5σ significant, i.e. there is a 1% probability that these two quantities are uncorrelated.

The ratio $L_{[CII]}/L_{[NII]}$ is fairly constant across a range of FIR colors but with a large scatter: $L_{[CII]}/L_{[NII]} = 9^{+6}_{-6}$ (Figure 3b). A proportionality between the two lines was also found in spatially resolved observations of the Milky Way (Bennett et al. 1994). We find an average ratio of $L_{[CII]}/L_{[NII]}$=9 in sources with [NII] detections, which agrees very well with the average empirical ratio in our galaxy (Wright et al. 1991, Bennett et al. 1994). However the many upper limits on [NII] indicate that many sources have larger $L_{[CII]}/L_{[NII]}$.

4.3. The [O I] (63 μm and 145 μm) Observations

The [O I] line at 63 μm is the second most commonly detected line in the present sample. It is detected in 46 of the 53 galaxies where it was observed. It is not detected in the [C II] deficient galaxies. Apart from these galaxies, $L_{[OI]}/L_{FIR}$ is unchanging with $F_\nu(60\ \mu m)/F_\nu(100\ \mu m)$. The mean value of $L_{[OI]}/L_{FIR} = 1.6 \times 10^{-3}$ with a standard deviation of about 50%, and the total range of values of roughly a factor of six (Figure 4). [O I] (145 μm) is fainter and was observed/detected only in a few galaxies.

The [O I](63μm) line is the other major coolant of neutral regions. Since the energy to excite this line is higher than for [C II] we expect this line to become more important relative to [C II] in warmer gas (i.e. higher G_0). This is indeed seen in Figure 5, where $L_{[OI]}/L_{[CII]}$ increases with $F_\nu(60\ \mu m)/F_\nu(100\ \mu m)$, indicating that warmer gas correlates with warm dust. In Figure 1 we saw that $L_{[CII]}/L_{FIR}$ decreases with $F_\nu(60\ \mu m)/F_\nu(100\ \mu m)$ and in Figure 4 we see that $L_{[OI]}/L_{FIR}$ does not decrease with $F_\nu(60\ \mu m)/F_\nu(100\ \mu m)$, so we should be able to predict the correlation seen in Figure 5. The generalized Kendall's rank test for the correlation between $L_{[OI]}/L_{[CII]}$ and $F_\nu(60\ \mu m)/F_\nu(100\ \mu m)$ gives a 5.5σ significance for a sample of 50 galaxies. This is the strongest correlation we see in this dataset, and there is a good physical reason for that. PDR models (e.g. Kaufman et al. 1999) show that both the increase in dust temperatures ($F_\nu(60\ \mu m)/F_\nu(100\ \mu m)$) and [O I](63 μm)/[C II](158μm) are due to an increase in FUV flux G_0. We make a detailed comparison between the PDR models and observations in the next section.

[O I](63 μm) does not dominate the cooling for the galaxies in the sample where $F_\nu(60\ \mu m)/F_\nu(100\ \mu m) \leq 0.8$. Therefore, if photoelectric heating is the dominant heating mechanism, $L_{[CII]}/L_{FIR}$ tracks the heating efficiency for the cooler galaxies [$F_\nu(60\ \mu m)/F_\nu(100\ \mu m) \leq 0.8$]. Total heating efficiency is given by the ratio $(L_{[CII]} + L_{[OI]})/L_{FIR}$ and decreases with $F_\nu(60\ \mu m)/F_\nu(100\ \mu m)$, as discussed in the next section.

The [O I](63 μm) line is optically thick in some cases. This can be seen by comparing it to the [O I](145 μm) line. The maximum allowed ratio in the optically thin limit $L_{[OI]145}/L_{[OI]63}$= 0.1 for $T > 300$K (TH85), whereas in the current sample $L_{[OI]145}/L_{[OI]63}$=0.18 for NGC 3620.

The $L_{[OI]145}/L_{[OI]63}$ line ratio can also be used to probe gas temperature; $L_{[OI]145}/L_{[OI]63}$ increases with gas temperature, but the S/N in the [O I] (145 μm) line is not enough in most galaxies where it is observed.

4.4. The [O III] (88μm and 52μm) lines

The [O III] line at 88μm is one of the more easily detected lines. We detect this line in 24 out of 34 galaxies where it was observed. Two low luminosity, irregular galaxies, NGC 1569 and IC 4662, with low values of L_{FIR}/L_B, have high values of $L_{[OIII]}/L_{FIR}$, with $L_{[OIII]}$ approaching or exceeding 1% of L_{FIR} (Figure 6). The [O III] (88 μm) line in these galaxies is stronger than the [C II] (158 μm) and [O I] (63 μm) lines from neutral gas. There is other evidence that the line and continuum emission in these galaxies may be dominated by H II regions (see Hunter et al. 2001 for details). There is relatively little dust near these H II regions, hence the low extinction, low L_{FIR}/L_B and high $L_{[OIII]}/L_{FIR}$. The irregular galaxies in the sample which are observed in [O III] have a high $L_{[OIII]}/L_{FIR}$.

The [O III] (52μm) line is not so widely detected, or observed, due to the relatively low sensitivity of the detector at those wavelengths. This line was detected in 3 out of 11 galaxies where it was observed.

5. Interpretation of the data

5.1. Electron densities derived from [O III] lines

For three galaxies, NGC 5713, NGC 1569, and NGC 4490, we use the measured ratio of the two [O III] lines, at 88 and 52 μm, to derive electron densities n_e using the semi-empirical treatment of Rubin et al. (1994) with an assumed H II region electron temperature $T_e = 10^4$ K. The results are fairly insensitive to the temperature assumed. The 52 μm upper limits in five other galaxies can be combined with the measurement of 88 μm line flux to yield upper limits on n_e (Table 3).

Table 3: n_e from [O III] line ratios

Galaxy Name	[O III] 88/[O III] 52	Log(n_e/cm^{-3})
NGC 0278	> 1.75	< 0.1
NGC 520	> 0.63	< 2.6
UGC 02855	> 0.54	< 2.7
NGC 1482	> 1.38	< 1.8
NGC 1569	1.55	1.5
NGC 4418	> 0.21	< 3.4
NGC 4490	1.25	2.0
NGC 5713	1.04	2.2

5.2. Variations in $L_{[CII]}/L_{FIR}$ and proposed explanations

In Paper I we discussed many possible reasons for the extremely low values of $L_{[CII]}/L_{FIR}$ observed in some galaxies. Some of these hypotheses can be ruled out with the observations of other FIR lines, the most prominent of these being [O I](63 μm) and the [NII] (122 μm). We review the various reasons proposed for the [C II] deficiency in Paper I and in Luhman et al. (1998) and discuss them in light of current observations.

(A) The [C II] line could be optically thick in emission. This hypothesis is supported by the compactness of the mid-IR emission in the three galaxies with the lowest $L_{[CII]}/L_{FIR}$. The [C II] line becomes optically thick at $N(C^+) = 5 \times 10^{17}\mathrm{cm}^{-2}$ for a velocity width of 4 km/s (Russell et al. 1980). Assuming a velocity width of 120 km/s for NGC 4418 (Sanders, Scoville & Soifer 1991) and $N(C^+)/N(H) \simeq 1.4 \times 10^{-4}$, optical depth of one in the [C II] line is reached for column densities of $N(H) = 8 \times 10^{22}$ cm^{-2}, or $A_V = 40$ in the PDR gas. The total extinction towards the nucleus of NGC 4418 is $A_V > 50$. This would imply an unusually high ratio of PDR to cold molecular gas.

The biggest uncertainty in estimating the column density of gas needed to produce optically thick emission is the velocity structure of the gas; if there is velocity crowding (e.g. near the center or in a bar) or if most of the self-absorption is local (i.e. in the same cloud or within a small velocity interval), even a small column density of gas can be effective. But large optical depths are difficult to produce because of the following argument. Models of PDRs, assuming that grain opacity and gas abundances both scale with metallicity, show that the column of C^+ in a PDR is only of order a few times 10^{17} so that the [C II] has optical depths in a given cloud only of order unity, unless every line of sight through the cloud goes through many PDRs. But in that case one would see emission from the first optical depth of unity, so for an optical depth of 100 in C^+, one would get 1/100th of the emission compared to the optically thin case (and not e^{-100}). So to explain $L_{[CII]}/L_{FIR}$ which is 100 times lower, one would need an optical depth of 100 in the PDRs, which corresponds to a hydrogen column density of $\simeq 3 \times 10^{23}\,\mathrm{cm}^{-2}$.

Another way to produce large optical depth is to have cold C^+ on the outside of the cloud while the PDR inside produces [C II] emission. The cold gas must then be turbulent enough to have a velocity width equal to or larger than the warm/emitting gas so that [C II] emission in the line wings does not escape. Self-absorption is seen in the 158μm line when observed at high spectral resolution (Boreiko & Betz 1997), and in ISO observations of Sgr B2 (Cox et al. 1999), but the line width of the cold gas is usually smaller than that of the warm gas, leading to a reduction in flux by a factor of roughly two, but cannot produce a factor of 60 reduction in flux without a good match in velocity widths.

Since [O I] is present up to higher optical depths in clouds than C^+, [O I] is more likely to have larger columns and to be self absorbed. Towards the Galactic center a deeper absorption profile is seen in the [O I] (63 μm) line (Keene et al. 1999, Cox et al. 1999, Poglitsch et al. 1996, Kraemer, Jackson & Lane, 1996) than in the [C II] line (Cox et al. 1999). [O I] should go optically thick *faster* than [C II] if optical depth were the reason for decreasing $L_{[CII]}/L_{FIR}$. Thus we should have seen a more dramatic decline in $L_{[OI]}/L_{FIR}$ than is seen in $L_{[CII]}/L_{FIR}$ with increasing $F_\nu(60\ \mu m)/F_\nu(100\ \mu m)$ or L_{FIR}/L_B. Since no decline is seen in $L_{[OI]}/L_{FIR}$ (Figure 4b), we discount self-absorbtion as the dominant reason for the decrease in $L_{[CII]}/L_{FIR}$.

(B) High dust extinction: For dust extinction to be important $\tau_{dust} = 1$ at 158 μm implies $A_V = 15,000$. This is still insufficient to explain the [C II] deficiency and is unlikely even for very obscured starbursts like Arp 220 (Fischer et al. 1999). Since the [O I] line at 63μm is at shorter wavelengths it is even more vulnerable to extinction effects but still requires far too high an A_V for this to be a viable explanation. We should have also seen a dramatic decrease in $L_{[OI]}/L_{FIR}$ with increasing L_{FIR}/L_B in figure 4b since L_{FIR}/L_B is a measure of extinction effects in galaxies, but such a trend is not seen.

(C) Softer radiation from older/less massive stellar populations could lead to lower $L_{[CII]}/L_{FIR}$ due to a lack of C-ionizing photons. If much of the grain heating is by longer wavelength photons, rather than by FUV, [C II] will be relatively weak compared to FIR because grain photoelectric heating of the gas will be inefficient. This can happen when dust heating is by old, low mass stars. Luhman et al. (1998) postulate this scenario for [C II]-deficient ULIRGs. An aging starburst and a weak UV field relative to a softer, optical/infrared field which heats the dust, is also used to explain the [C II] line weakness in the Galactic center (Nakagawa et al. 1995). This mechanism seems unlikely to explain the most dramatic [C II] deficiency systematically found in galaxies with warmer FIR colors and higher L_{FIR}/L_B ratios, with the hotter dust pointing to the presence of massive stars and UV photons. It also seems unlikely that all starbursts are old by the time we see them. This explanation is more likely for the decrease seen in $L_{[CII]}/L_{FIR}$ in early type galaxies with low rates of star formation and the lowest L_{FIR}/L_B in the sample (to the left extreme of Figure 1b; also see Malhotra et al. 2000). Softer radiation fields in early type galaxies then lead to somewhat lower (by factors of a few) $L_{[CII]}/L_{FIR}$; this is corroborated by lower values of [C II]/CO seen in one of these galaxies (Malhotra et al. 2000).

(D) An obscured AGN can lead to both higher L_{FIR}/L_B and lower $L_{[CII]}/L_{FIR}$. This hypothesis is supported by the observed compactness of the [C II]-deficient sources in the mid-IR (Dale et al. 2000). A buried AGN could produce a small $L_{[CII]}/L_{FIR}$ since the UV field is inefficient at making [C II], both due to its hardness (higher ionization states for C

will be common) and due to its overall strength (see (F) below). This explanation may not hold for the ULIRGs, e.g. Arp 220, which are now believed to be powered by starbursts (Genzel et al. 1998). The AGN hypothesis may explain the deficiency of [C II] but does not easily explain the trends in $L_{[CII]}/L_{FIR}$ with L_{FIR}/L_B and $F_\nu(60\ \mu m)/F_\nu(100\ \mu m)$ unless a significant fraction of galaxies have obscured active nuclei, and even then one would expect the AGNs to add more scatter than a trend.

(E) For high values of G_0 (or T) and n, [O I] (63μm) emission is stronger than [C II] emission, since [C II] is quenched by collisional de-excitation. The grain charge, which determines the gas heating efficiency as measured by the observed ratio $(L_{[CII]} + L_{[OI]})/L_{FIR}$, is set by G_0/n. Therefore, with G_0/n fixed, raising G_0 and n together does not change $(L_{[CII]} + L_{[OI]})/L_{FIR}$, but it does increase $L_{[OI]}/L_{[CII]}$ and $L_{[OI]}/L_{FIR}$ while decreasing $L_{[CII]}/L_{FIR}$. In other words, the heating efficiency stays constant, but the cooling increasingly emerges in the [O I] line instead of the [C II] line as G_0 rises with G_0/n fixed. In section 4.3, we observed that the ratio of the two major cooling lines of the neutral ISM, $L_{[OI]}/L_{[CII]}$, increases with increasing $F_\nu(60\ \mu m)/F_\nu(100\ \mu m)$ (Figure 5). $F_\nu(60\ \mu m)/F_\nu(100\ \mu m)$ is a rough indicator of the dust temperature and increases with the FUV flux G_0. Since the [O I] (63μm) line has an excitation energy $\Delta E/k$=228 K compared with $\Delta E/k$=92 K for the [C II] (158μm) line, an increase in gas temperature caused by an increase in G_0 will increase $L_{[OI]}/L_{[CII]}$. Therefore, the correlation between $L_{[OI]}/L_{[CII]}$ and $F_\nu(60\ \mu m)/F_\nu(100\ \mu m)$ is likely due to an increase in G_0, which increases both gas and dust temperatures. However, Figure 7 shows that $(L_{[CII]} + L_{[OI]})/L_{FIR}$ does *not* stay constant with increasing $F_\nu(60\ \mu m)/F_\nu(100\ \mu m)$ or increasing G_0. This is a clear indication that the density is not rising as rapidly as G_0 and that grains are becoming more positively charged. Therefore this hypothesis, although it may contribute somewhat to the [C II] deficiency, cannot be the dominant cause.

(F) For high ratios of FUV flux to gas density (G_0/n), the dust grains become highly positively charged and are less efficient at heating the gas because of a higher potential barrier to photoelectric ejection (TH85). Hence there is less total gas cooling relative to the FIR continuum emitted by grains. For example, increasing G_0 while keeping n fixed raises the grain charge, lowers the gas heating efficiency $(L_{[CII]} + L_{[OI]})/L_{FIR}$, lowers $L_{[CII]}/L_{FIR}$ and raises $L_{[OI]}/L_{[CII]}$. An increase in G_0, accompanied by an increase in G_0/n, is the likely explanation for the trend of decreasing $(L_{[CII]} + L_{[OI]})/L_{FIR}$ with $F_\nu(60\ \mu m)/F_\nu(100\ \mu m)$ seen in Figure 7, as the dust gets warmer with increasing G_0 and more positively charged with increasing G_0/n. In addition, it accounts for the decrease in $L_{[CII]}/L_{TIR}$ with $F_\nu(60\ \mu m)/F_\nu(100\ \mu m)$ seen in the data plotted in Figure 9. This, then, is our favored hypothesis; in the next section we compare PDR models to $L_{[CII]}/L_{FIR}$ to further bolster this hypothesis.

5.2.1. [C II] deficiency Case Study: Arp 220

Of the explanations suggested above, (C) & (F) postulate a decrease in neutral gas heating relative to grain heating. In the others, either [C II] is attenuated by dust (B) or the cooling emerges in other lines (A, D and E). We have already ruled out E (cooling by [O I]) as the dominant cause of the reduction in $L_{[CII]}/L_{FIR}$. We can further test hypotheses A and D by measuring the emission in all the major cooling lines to see which, if any, line has replaced [C II] and [O I] as the coolant of the neutral medium. The total cooling budget can then be computed to see if the heating efficiency has declined. (The test is less stringent for D, since the gas cooling may be predominantly in optical lines which are absorbed by dust and emerge as continuum.)

At present Arp 220 is the only [C II] deficient galaxy for which a relatively complete census of gas cooling lines has been made. Gerin and Phillips (1998) have observed this galaxy in the [CI] (492 GHz) line and higher-lying CO rotational lines, and Sturm et al. (1996) observed this galaxy in H_2 rotational lines. Table 4 summarizes the energy output in cooling lines of neutral gas in Arp 220.

Table 4: Arp 220: Energy Budget

	Flux (observed) (W/m^{-2})	Flux(extinction corrected) (W/m^{-2})
FIR Continuum [1]	6.8×10^{-12}	
[C II] [1]	8.7×10^{-16}	
CI ($^3P_1$-$^3P_0$) [1]	1.9×10^{-17}	
CI (total) [1]	1.0×10^{-16}	
CO (1-0) [1]	1.8×10^{-18}	
CO (total) [1]	2.1×10^{-16}	
H_2 S(5) [2]	2.4×10^{-16}	2.4×10^{-15}
H_2 S(2) [2]	$< 1.5 \times 10^{-16}$	$< 7.0 \times 10^{-16}$
H_2 S(1) [2]	2.3×10^{-16}	9.7×10^{-16}
H_2 S(0) [2]	$< 3.5 \times 10^{-16}$	$< 7.3 \times 10^{-16}$

[1] Gerin & Phillips 1998

[2] Sturm et al. 1996

We see that only the molecular hydrogen lines come close to matching even the reduced output in [C II]. [O I] (63μm) is seen in absorption (Fischer et al. 1999). We conclude that there is a reduced ratio of gas heating to grain heating in at least this [C II] deficient galaxy. This is then consistent with hypotheses C and F.

5.3. Trends in $L_{[CII]}/L_{FIR}$: comparison to the PDR models

Of the various explanations for the trends and the deficiency of $L_{[CII]}/L_{FIR}$ listed above, the data most favor scenario (F) where the decrease in $L_{[CII]}/L_{FIR}$ is due to reduced heating via charged grains at higher values of G_0/n, with scenario (E) contributing to the decrease in [C II] luminosity when [O I](63 μm) starts dominating ($F_\nu(60\ \mu m)/F_\nu(100\ \mu m) \geq 0.8$). In Figure 9a and 9b we see the quantitative comparison of $L_{[CII]}/L_{FIR}$ and $L_{[OI]}/L_{FIR}$ with the PDR models of Kaufman et al. (1999). The term PDR refers to the neutral ISM in galaxies, including diffuse clouds or cold neutral medium (CNM), warm neutral medium (WNM), dense neutral gas around H II regions and molecular clouds illuminated by the interstellar radiation field (ISRF). PDRs are formed wherever FUV photons play a dominant role in the heating and chemistry of the gas.

In order to compare the data to the models we need to correct the quantity L_{FIR} used previously to include the dust emission outside the wavelength range 40-120μm. Since the long wavelength part of the dust emission ($\lambda > 120\mu$m) is not measured for these galaxies, we have to rely on dust emission models based on Galactic dust and other well-studied galaxies. Empirical data from IRAS and ISO indicate that the overall spectral shape in the infrared may be represented to first order as a function of one parameter, the $F_\nu(60\ \mu m)/F_\nu(100\ \mu m)$ ratio. Dale et al. (2001) have proposed a single parameter family of spectral energy distributions (SEDs) based on those data from which we convert FIR (dust emission in the 40-120μm) to total infrared emission (TIR; 3-1100 μm), including emission from PAHs and dust associated with cold cirrus. The uncertainty in converting FIR to TIR is about 15% (D. Dale, private communication).

Two things are apparent from this comparison. First, the PDR models do reproduce the decrease in $L_{[CII]}/L_{TIR}$ with $F_\nu(60\ \mu m)/F_\nu(100\ \mu m)$. For the extremely deficient $L_{[CII]}/L_{TIR}$ galaxies, the PDR models of Kaufman et al. (1999) require $G_0/n > 10^2\, cm^3$ in order for $L_{[CII]}/L_{TIR} < 10^{-4}$. We note in Figure 8 that a second PDR solution for $L_{[CII]}/L_{TIR} < 10^{-4}$ occurs for a much higher G_0/n ratio. However, this solution produces far more $L_{[OI]}$ than is observed; it is essentially hypothesis (E) ruled out from the last section. In the regime $G_0/n > 10^2\, cm^3$, radiation pressure on grains may drive them through the gas at large drift velocities, resulting in additional gas heating, a detail not considered in the Kaufman et al. (1999) models; recent calculations by Weingartner & Draine (1999) show that such grain drift will only be important for large grains, while small grains, which are responsible for gas heating and much of the FUV absorption in the PDR models, will not be significantly affected.

Second, we note in Figure 8 that about half the galaxies have $L_{[CII]}/L_{TIR}$ which is too high by a factor of about two to be explained by PDR models with any parameters.

This is not very surprising, since not all of the [C II] comes from PDRs; ionized gas in diffuse ionized regions can contribute significantly to [C II] emission as well (Petuchowski & Bennett 1993, Heiles 1994). We discuss this further in the next section.

5.4. [C II]/[NII](122 μm) from ionized regions

The ionized gas contribution to [C II] can be estimated from measurements of the [NII] (122 μm) line, which arises exclusively in the ionized gas. For the asymptotic high electron density limit ($n_e >> n_{crit}$, where $n_{crit} = 3.1 \times 10^2 \mathrm{cm}^{-3}$ for [NII](122 μm) and $n_{crit} = 50\,\mathrm{cm}^{-3}$ for [C II](158μm)) (see Table 1):

$$\frac{\mathrm{L_{[CII]}}}{\mathrm{L_{[NII]}}} = 0.288 \frac{N(C^+)}{N(N^+)}$$

where $N(N^+)$ and $N(C^+)$ are the numbers of the respective ions, and the Einstein A coefficients used are $A_{158} = 2.3 \times 10^{-6} s^{-1}$ (Froese-Fischer & Saha 1985) and $A_{122} = 7.4 \times 10^{-6} s^{-1}$ (Froese-Fischer 1983).

In the low density limit ($n_e << n_{crit}$) the ratio is given by:

$$\frac{\mathrm{L_{[CII]}}}{\mathrm{L_{[NII]}}} = 3.05 \frac{N(C^+)}{N(N^+)}$$

where the collision strengths are taken to be $\Omega_{12} = 2.15$ (Blum and Pradhan 1992) and $\Omega_{13} = 0.272$ (Lennon and Burke 1994).

The ratio of the [C II](158μm) and [NII](122μm) luminosities depends on the gas phase abundances of these ions. We expect the C^+ and N^+ abundances to be different in different galaxies in the sample. At present, the abundances in these galaxies are not known so we use Galactic (Solar, or interstellar) abundances. Even in the Galaxy the differences are substantial: $[C/H] = 1.4 \times 10^{-4}$ in absorption line measurements of diffuse gas (Sofia et al. 1997) and $[C/H] = 2.4 \times 10^{-4}$ (Esteban et al. 1998, Rubin et al. 1993) as measured in emission in Orion. Nitrogen abundances are less discrepant: $[N/H] = 7.5 \times 10^{-5}$ from absorption line measurements of the diffuse gas (Meyer et al. 1997) and $[N/H] = 6.8 \times 10^{-5}$ from emission line studies in Orion (Esteban et al. 1998, Rubin et al. 1993). For various combinations of those abundances, the expected $\mathrm{L_{[CII]}}/\mathrm{L_{[NII]}}$ ranges from 5.7 to 10.7 in the diffuse ($n << n_{crit}$) limit and from 0.54 to 1.0 for dense ionized gas ($n >> n_{crit}$). Furthermore, combining the abundances observed in the diffuse ionized gas (DIG) with the diffuse gas estimates points to 5.7 as the most reasonable value to adopt.

In the galaxies where both lines are detected, $L_{[CII]}/L_{[NII]}$ ranges from 4.3-24, and including upper limits increases the range to 4.3-29. The geometric mean of $L_{[CII]}/L_{NII}$ ratio in the sub-sample where both lines are detected is 8, and the arithmetic mean in 9.

The total [C II] in a galaxy comes from PDRs, DIG and H II regions, whereas the [NII] arises from DIG and H II regions. Thus the variable fractions of the galaxy's ISM involved in each of those components will add scatter to $L_{[CII]}/L_{[NII]}$, as will variations in C and N abundances. Using a constant multiplied by the [NII] flux to correct the [C II] flux for ionized region contributions is therefore an oversimplification we adopt in the absence of further information on individual galaxies. The observed values of $L_{[CII]}/L_{[NII]}$ cluster clearly near the low end, with more than half between 4.5 and 6, suggesting that the most generally applicable correction to [C II] must be near the lower end of that histogram as well. This also favors the ratio of 5.7 based on the lower abundance of C^+, which we adopt in what follows.

The amount of [NII] emission from diffuse versus dense regions has only been measured for the Milky Way. From FIRAS measurements of the two [NII] lines at 205 and 122μm in the Milky Way, Bennett et al. (1994) conclude that most of the emission is from diffuse gas. The predicted ratio of these lines is I(122)/I(205)=0.7 for diffuse gas ($n_e << 100\,\mathrm{cm}^{-3}$), and I(122)/I(205)=3 for $n_e \simeq 100\mathrm{cm}^{-3}$ (Rubin 1985). Taking the middle of the range of the observed ratio I(122)/I(205)=1.0 to 1.6 (Wright et al. 1991), about 75% of [NII] emission comes from diffuse gas. This implies that [C II] emission from the ionized medium $[CII]_{ion} = 4.3 \times [NII](122)$. We will therefore approximate the [C II] flux from PDRs as $[CII]_c = [CII] - 4.3 \times [NII](122)$ in what follows.

The mean and median adjustment made in the [C II] flux to thus remove the ionized gas contribution is roughly 50%. This estimate agrees with a similar estimate by Petuchowski & Bennett (1993) for the contribution to the Milky Way [C II] by the warm ionized medium. This is not surprising since we have used Galactic abundance ratios, and the average $L_{[CII]}/L_{[NII]}$ in this extragalactic sample agrees with the Milky Way value. We believe that while statistically this may be a reasonable treatment to estimate the ionized gas contribution to [C II], it may be inaccurate for at least some individual galaxies because of variations in C/N abundance ratios and in the fraction of diffuse and dense ionized gas. In Section 6.1, we check for and discuss the accuracy of estimating $[\mathrm{C\ II}]_c$.

5.5. [O I]/[C II] compared to PDR models

In section 4.3, we noted a strong correlation between the ratio of the two PDR cooling lines [O I](63 μm)/[C II](158 μm) and far-infrared colors, $F_\nu(60\ \mu m)/F_\nu(100\ \mu m)$. The increase in $L_{[OI]}/L_{[CII]}$ is due to the drop in $L_{[CII]}$ compared with L_{FIR} and not due to an increase in $L_{[OI]}/L_{FIR}$.

Qualitatively, this trend can be explained by postulating that both the increase in $L_{[OI]}/L_{[CII]}$ and $F_\nu(60\ \mu m)/F_\nu(100\ \mu m)$ come about in PDRs as a result of increase in the average FUV flux G_0. The overall decrease of $(L_{[CII]} + L_{[OI]})/L_{FIR}$ (Figure 7) means that G_0/n is also increasing. In PDR models, increasing G_0 leads to an increase in the grain temperature and therefore an increase in $F_\nu(60\ \mu m)/F_\nu(100\ \mu m)$. Increasing G_0 also raises the gas temperature which raises the ratio $L_{[OI]}/L_{[CII]}$. Figure 9 shows a quantitative comparison between the observations and the PDR models of Kaufman et al. (1999). While the models run parallel to the trends seen, the observed $L_{[OI]}/L_{[CII]}$ is too high compared to the models. Some of this could be due to [C II] flux from ionized gas.

When the contribution from ionized gas is subtracted using [NII] (122 μm) line measurements as discussed in the last section, the models and the data show better agreement. In addition, by using the corrected, $[C\ II]_c$, in $L_{[OI]}/L_{[CII]}$, we see that the increase in $L_{[OI]}/L_{[CII]}$ is due to an increase in both FUV flux. Comparison with PDR models (Figure 9b) shows that for $n = 10 - 10^3 cm^{-3}$ the increase in $L_{[OI]}/L_{[CII]}$ is due to an increase in G_0, but for $n > 10^3 cm^{-3}$ the $L_{[OI]}/L_{[CII]}$ increases due to an increase in both G_0 and n. The critical density for [C II] is $3 \times 10^3\,cm^{-3}$, while for [O I] it is $5 \times 10^5\ (T/300)\,cm^{-3}$. It is interesting, then, that $L_{[OI]}/L_{[CII]}$ shows a good correlation with the FIR color, which does not depend on n but on G_0 alone. In the next section we will present more evidence that G_0 and n tend to increase together.

6. Physical Conditions in the PDRs

After subtracting an estimated fraction of [C II] line flux that arises in ionized gas, we are left with [C II] line flux arising from PDRs. To derive the physical conditions of PDRs we compare the observed line ratios and line to continuum ratios with a grid of recent detailed PDR models by Kaufman et al. (1999) which take into account the chemistry, heating and cooling in PDRs. These models calculate the line emission in [C II](158μm), [O I] (63 μm and 145 μm), and dust continuum emission for a plane slab of gas illuminated from one side by FUV. Gas heating is dominated by photoelectrons ejected from classical (i.e. big, spherical) grains, and from PAHs following the treatment by Bakes and Tielens (1994).

Including the effects of PAH photoelectric emission raises the PDR surface temperatures by as much as a factor of 3 compared to the previous PDR models (e.g. WTH).

The comparison of measured fluxes of [C II] (158μm) and [O I] (63 μm) lines to the PDR model predictions allows us to infer the physical conditions in the PDRs, primarily gas density n and FUV flux G_0. This method may not give the right answers if: (1) the various lines and the continuum arise from different locations in the galaxies; (2) if there is self-absorption of the lines from cold gas outside the PDRs where they originate. [O I] (63 μm) is most susceptible to this, and we try to correct for it in the models as described below.

The PDR models are used to calculate the emergent flux from the front face of a plane parallel slab of gas illuminated from one side. A galaxy has many PDRs at all orientations, and optical depth effects are non-negligible. In the approximation that most dense PDRs are the shells of molecular clouds, and that the [C II] line and dust continuum emission are optically thin whereas [O I](63 μm) is optically thick, [O I] is seen only from the front side of each cloud and [C II] and FIR from both the front and the back sides. The velocity dispersion from cloud to cloud however allows most [O I] (63μm) photons that have escaped their parent cloud to escape the galaxy entirely. This scenario implies that we should observe only half of the [O I] flux and all of the [C II] and dust continuum flux expected from PDR models. This adjustment has been applied hereafter to the PDR model predictions.

Figure 10(a) shows the measured ratios $L_{[OI]}/L_{[CII]_c}$ and $(L_{[OI]} + L_{[CII]_c})/L_{TIR}$ compared with the values obtained from a grid of PDR models with various values of G_0 and n. With just these two measured ratios there are two possible regimes of G_0 and n which reproduce the observed values. One of the regimes is shown in Figure 10(a), while the other is a high n ($10^4\,\mathrm{cm}^{-3} < n < 10^5\,\mathrm{cm}^{-3}$), low G_0 ($G_0 \simeq 1$) regime. To distinguish between the two, we need to reliably measure the ratio $L_{[OI]145}/L_{[OI]63}$. This measurement is not available for most of the galaxies in this sample, [O I](145 μm) being too faint. However the high n, low G_0 solution does not reproduce the line fluxes measured, i.e. the fluxes in the [C II] line fall short by about 2 orders of magnitude when $10^4 < n < 10^5$ and $G_0 \simeq 1$ compared to the observed values. This is not to say that such high density, low radiation environment (e.g. molecular clouds) do not exist in galaxies, they simply do not contribute much to the observed fluxes seen in [O I], [C II] lines and the FIR continuum.

6.1. G_0 and n from [O I]/TIR values

We can also use the $L_{[OI]}/L_{TIR}$ ratio to derive G_0 and n by comparing the observed $L_{[OI]}/L_{TIR}$ vs. $F_\nu(60\ \mu m)/F_\nu(100\ \mu m)$ with models. Such a comparison, shown in Figure 11(b), using models by Kaufman et al. (1999), suggests that the constancy of [O I]/FIR (or TIR) against variations in $F_\nu(60\ \mu m)/F_\nu(100\ \mu m)$ implies a simultaneous increase in both gas density n and FUV flux G_0. The model $F_\nu(60\ \mu m)/F_\nu(100\ \mu m)$ ratio for a given UV flux G_0 is calculated following the treatment by Hollenbach, Takahashi & Tielens (1991). The 60 and 100 μm fluxes are calculated assuming classical grains in thermal equilibrium. For low G_0, the emission from classical grains is from the Wein side of the blackbody curve, and the $F_\nu(60\ \mu m)/F_\nu(100\ \mu m)$ is set by stochastically heated grains. This has the effect of yielding essentially the same $F_\nu(60\ \mu m)/F_\nu(100\ \mu m)$ for $G_0 = 1 - 10^{2.5}$. The other uncertainty in using $L_{[OI]}/L_{TIR}$ to derive G_0 and n is that [O I](63 μm) may be optically thick; we have accounted for this by reducing $L_{[OI]}/L_{TIR}$ from the models by a factor of two, as before. An advantage to this disagnostic however is that we avoid uncertainties associated with correcting for the [C II] flux from ionized regions.

Figure 11 compares the G_0 and n values obtained using each set of observables, $L_{[OI]}/L_{[CII]_c}$ vs $(L_{[OI]} + L_{[CII]_c})/L_{TIR}$ and $L_{[OI]}/L_{TIR}$ vs $F_\nu(60\ \mu m)/F_\nu(100\ \mu m)$. The difference in $\log(G_0)$ obtained by these two methods $\Delta Log(G_0)$ shows a mean of 0.08 and $\Delta log(n)$ shows a mean of 0.06. Thus there is no indication that one method yields systematically higher or lower values of G_0 or n. From the absolute values of ΔG_0 and Δn, we infer that for half the galaxies G_0 and n values from the two methods agree to better than a factor of 2 and 1.5, respectively. This difference may be taken as an estimate of uncertainty in the derived values, which is sensitive to some measurement errors (one method uses only the [O I] line while the other uses [C II], [O I] and [NII]) and to some sources of systematic errors (for example, subtraction of the ionized gas contribution to [C II] flux), but not to all possible systematics. For instance, this estimate would not be sensitive to uncertainties in the abundances used in the models, or to the assumption that about half the dust heating is due to FUV photons, or to the fact that we measure luminosity weighted averages of line and continuum contributions emanating from many parcels of ISM with different physical conditions.

6.2. Discussion and interpretation

The average physical conditions in this sample of normal galaxies are FUV flux $G_0 = 10^2 - 10^{4.5}$ and gas densities $n = 10^2 - 10^{4.5}\,cm^{-3}$. The derived values of G_0 and n follow a trend with $G_0 \propto n^\alpha$, $\alpha = 1.3$ or 1.4 (Figure 12). This may be evidence for a

Schmidt law on fairly local scales in the galaxies, where high gas densities correlate with high star formation rates (Schmidt 1959) and agrees with the recent determinations by Kennicutt (1998) where the surface densities of star-formation and gas scale by an exponent N=1.4: $\Sigma_{SFR} \propto \Sigma_{gas}^{1.4}$. The observed scaling between G_0 and n may be also dictated simply by geometry if the FIR line and continuum emission is dominated by regions near young stars. From simple Strömgren sphere calculations (cf. Spitzer 1978) we can derive that the FUV flux at the neutral surface just outside the Strömgren sphere should scale as $G_0 \propto n^{4/3}$, which is consistent (within errors) to the scaling seen in Figure 11.

We favor the latter interpretation primarily because it is the more direct one. The Schmidt law applies to surface density or a density which is averaged over the entire galactic disk thickness. It reflects the physics that on a *global* scale, the star formation rate may scale as the mass (density) or, if cloud collisions are important, for example, on a higher power of the mass (density). However, the high values of G_0 and n which we derive make it clear that we are probing a very local phenomenon. We are not probing the rate of star formation in as much as the typical distance from an OB star or OB association to a PDR which absorbs its FUV photons. O and early B stars form in dense cores within giant molecular clouds (GMCs), whose diameters are of order 10–50 pc. For a fraction of their lives, the OB stars are embedded in the clouds, surrounded by very dense and compact H II regions and PDRs illuminated by intense UV fluxes. Later, the expanding H II regions break through the surfaces of the clouds, champagne flows are created, and eventually the OB stars lie outside, but close, to their natal GMCs. To produce a flux of $G_0 \approx 1000$ on the surface of that cloud, an O7 star must be only about 1 pc distant. With a relative speed of 1 km/s with respect to the cloud, an O star travels only 1 pc in 10^6 years, a substantial portion of its lifetime. Therefore, the FUV photons from OB stars tend to be absorbed in two very different environments. A substantial fraction (McKee & Williams 1997 estimate $\geq 30\%$ for the Lyman continuum photons) are absorbed in their immediate vicinity - in the GMC of their birth. The rest escape from the natal cloud and travel through the diffuse ISM to be absorbed primarily by diffuse gas at distances of order 100–300 pc, with much lower values of G_0 and n ($\sim$2 and 100 cm^{-3} in the local ISM of the Milky Way). These two components are consistent with the decomposition of the FIR dust emission into "active" and "cirrus" components by Helou (1986). [C II] (158μm) can have significant contributions from the DIG, the diffuse neutral gas, and the locally irradiated PDRs of the natal GMCs. [O I] (63μm) is dominated by emission from the PDRs of the natal GMCs. The PDR modeling procedure provides an average of these two components, weighted to the high G_0 and high n GMC component. The simple Strömgren sphere scaling $G_0 \propto n^{4/3}$ applies directly to this GMC component, and should therefore manifest itself in the integrated fluxes as seen in Figure 12.

The derived PDR pressures [10] also lend credence to the view that the $G_0 \propto n^{1.4}$ correlation arises from the correlation of n and G_0 in an expanding H II region surrounded by a PDR. In such a picture, the H II region thermal pressure should approximately equal the PDR thermal pressure. The thermal pressure in the H II regions can be estimated from the electron density derived from [O III] (88μm)/[O III] (52μm) ratio if both lines are observed (Rubin et al. 1994). This comparison was made for the three galaxies in our sample with measurements of the [O III] lines. The pressures derived for H II regions are tabulated in Table 7. The H II region and PDR pressures agree to roughly a factor of two in all cases (assuming $T_e = 8000K$).

The derived temperatures at the PDR surfaces range from 270-900 K, and the pressures range from $6 \times 10^4 - 1.5 \times 10^7\,\mathrm{K\,cm^{-3}}$ (Table 6). The lower value of the pressure range is roughly twice the local solar neighborhood value and the upper end is comparable to pressures in H II regions in starburst galaxies (Heckman, Armus & Miley 1990) which also corresponds to the pressure and surface brightness at which starbursts saturate (Meurer et al. 1997).

Figure 12 shows that the thermal gas pressures increase with grain temperatures, or the flux of photons incident upon the absorbing grains. This is mainly due to the $L_{[OI]}/L_{[CII]}$ vs $F_\nu(60\ \mu\mathrm{m})/F_\nu(100\ \mu\mathrm{m})$ correlation in Figure 5. Higher values of $L_{[OI]}/L_{[CII]}$ imply higher G_0 and gas densities, and therefore higher pressures. The temperature of the gas also increases with $F_\nu(60\ \mu\mathrm{m})/F_\nu(100\ \mu\mathrm{m})$ and contributes to the increase in pressure, but the increase in the gas density n is the more dramatic of the two. This too is explicable in terms of the local absorption of photons by the expanding H II regions and associated PDRs in the natal GMCs of OB stars. Whether grains absorb most of the flux in the H II region or in the neighboring PDR, the photons will be absorbed at roughly R_S, the Strömgren radius for that star. If ϕ_i is the Lyman continuum photon luminosity of the star, then the photon flux is proportional to $\phi_i/R_S^2 \propto n_e^{4/3} \propto P_{\mathrm{HII}}^{4/3} = P_{\mathrm{PDR}}^{4/3}$, assuming pressure equilibrium between the H II gas and the PDR regions associated with them. Since the grain temperature scales roughly as the photon flux to the $1/5^{\mathrm{th}}$ power (Hollenbach, Takahashi & Tielens 1991), $T_{gr} \propto P_{\mathrm{PDR}}^{4/15}$.

We show a simple model to help explain the observed correlation between the FUV field strength, G_0, and the PDR pressure, P. If we assume that PDR gas is illuminated by hot stars in star clusters, then there is an approximate natural scaling between the FUV flux from stars in the cluster, the H II region density, and the pressure at the H II

[10]The PDR pressure is calculated as $P = nkT$ where gas density n and temperature T are derived from PDR models (see Kaufman et al. 1999 for details)

region/PDR interface. Assuming that all of the FUV flux emerges from one star of a given spectral type which has a bolometric luminosity, L_{bol} and which produces $S = 10^{49} S_{49}$ photons s^{-1} of ionizing photons, the size of the surrounding H II region, R_s is set by the number of ionizing photons and the electron density in the H II region. Assuming further an electron temperature, $T_e = 10^4\,\mathrm{K}$, the combination $n_e T_e$ sets the H II region pressure. Then, for a given bolometric stellar flux, the value of G_0 at the PDR surface is determined by $G_0 = L_{bol}/4\pi R_s^2$. If there is a pressure equilibrium at the H II region/PDR interface, then we find a correlation between G_0 and P. This is plotted as a correlation between $F_\nu(60\ \mu\mathrm{m})/F_\nu(100\ \mu\mathrm{m})$ and P (Figure 13). The calculations use three different spectral types (O5, O9, and B3) and electron densities ranging from 10^1 to $10^8\,\mathrm{cm}^{-3}$. Zero-age main sequence values of L_{bol} and S_{49} for the various spectral types are from Parravano (private communication).

Because the ISO-LWS beam views an entire galaxy for our sample galaxies, it incorporates many tens to hundreds of thousands of O and early B stars, with their associated H II regions and PDRs. As discussed above, the G_0, n and P we derive for a given galaxy represent an average value, weighted to the dense natal GMCs which lie close to the OB stars. The range of the G_0, n and P for the different galaxies can reflect several interesting differences in their star formation processes and histories. If global star formation in normal galaxies occurs in bursts, rather than continuously, then those galaxies which are observed shortly after their bursts ($\lesssim$ few million years) will show high G_0, n and P because the OB stars will not have had time to travel very far from their natal clouds. This hypothesis, however, requires the star formation bursts to be of significant amplitude, resulting in sustantially different instantaneous mass distributions of ionizing stars among galaxies.

The differences in G_0, n and P may instead reflect differences from galaxy to galaxy in the GMCs which form the OB stars. For example, larger GMCs may keep their OB stars embedded for a longer fraction of their lifetime, resulting in higher average G_0 and n. We note that n is the density in the PDR, which can be considerably higher than the average density in the GMC. On the other hand, the GMCs could be the same size but denser. In this scenario, the higher density ambient gas would lengthen the embedded phase of the OB star, and result in higher average G_0 and n. In either case, the galaxies with higher derived G_0 and n would contain more massive GMCs, on average.

7. Summary and Conclusions

In this paper we have attempted to understand the energetics and the physical conditions in a statistically representative set of star-forming normal galaxies by studying the atomic and ionic fine structure lines in the far-infrared. Such sensitive observations of a large sample were made possible by having a cryogenically-cooled observatory, ISO (Kessler et al. 1996), in space. The sample was selected to span a range in properties such as morphology, FIR colors $F_\nu(60\ \mu m)/F_\nu(100\ \mu m)$ (indicating dust temperatures), and L_{FIR}/L_B (indicating star-formation activity and optical depth). For a randomly drawn sample of galaxies, many of these parameters are correlated. Care was taken to span the full range of parameter space as much as possible in this sample. Still, there remains some correlations between these parameters. Galaxies with high L_{FIR}/L_B also tend to have warmer FIR colors and tend to be luminous.

Since this sample is more extensive than previous studies, many effects were seen for the first time. Among the more remarkable was the non-detection of [C II] line in two normal galaxies indicating low $L_{[CII]}/L_{FIR}$, down to 2×10^{-4} (3-σ upper limits). Lower ratios have been seen in association with Galactic H II regions, but such low ratios were unexpected in normal galaxies where the emission is from a mixture of sources: H II regions, WIM, and PDRs. Previous observations of galaxies had found $L_{[CII]}/L_{FIR}$ to vary little, between 10^{-2} and 10^{-3}. This result may have been biased because of the low sensitivity of the previous surveys and the selection criteria for the galaxies. DIRBE observations of the Milky Way also showed a spatially constant ratio $L_{[CII]}/L_{FIR}=3 \times 10^{-3}$, except in the Galactic center. In the current sample of normal galaxies we see a smooth decline in $L_{[CII]}/L_{FIR}$ with increasing dust temperature and star-forming activity in galaxies. In a sample of 60 normal galaxies, this trend spans a factor of more than 50 in $L_{[CII]}/L_{FIR}$ with [C II] deficient galaxies at the hottest and most active end. The anticorrelation between $L_{[CII]}/L_{FIR}$ and $F_\nu(60\ \mu m)/F_\nu(100\ \mu m)$ is the strongest, followed by $L_{[CII]}/L_{FIR}$ vs. L_{FIR}/L_B. The anticorrelation between $L_{[CII]}/L_{FIR}$ and the IR-luminosity is the weakest and may be a secondary correlation. This is good news for searches for distant startbursts. The most luminous galaxies are not necessarily [C II] deficient: warm galaxies are more likely to show a lower $L_{[CII]}/L_{FIR}$, whereas cool luminous galaxies can be detected.

There have been many explanations for the variations in $L_{[CII]}/L_{FIR}$, but on examining the evidence we favor the scenario where $L_{[CII]}/L_{FIR}$ decreases as the heating of the gas becomes less efficient in the high G_0/n regime due to charging of dust grains. As the grains become positively charged the efficiency of photoelectric ejection decreases. The various lines of evidence supporting this hypothesis are:
(1) $L_{[CII]}/L_{FIR}$ deficiency is seen in the more actively star-forming galaxies with warmer

FIR colors.
(2) Examination of heating and cooling balance in Arp 220 does not show any other lines that could be cooling the neutral ISM instead of [C II]. In our own sample, the inclusion of [O I] does not change the low ratio of gas to grain heating as indicated by $(L_{[CII]} + L_{[OI]})/L_{FIR}$. So far we have failed to identify other channels, which leads us to believe that heating efficiency is low in galaxies where where $L_{[CII]}/L_{FIR}$ is low.
(3) PDR models which include grain charging and the photoelectric effect successfully reproduce the trends of decreasing $(L_{[CII]} + L_{[OI]})/L_{FIR}$ and $L_{[CII]}/L_{FIR}$ with $F_\nu(60\ \mu m)/F_\nu(100\ \mu m)$ (Figure 8).

The [C II] line flux shows better correlation (and less scatter) with mid-IR flux from galaxies which is dominated by aromatic features and emission from transiently heated small grains (Helou et al. 2001). This indicates that the heating of gas is dominated by such grains as expected by some theoretical considerations (e.g. Bakes & Tielens 1994).

A somewhat less dramatic decrease in $L_{[CII]}/L_{FIR}$ is seen in early type galaxies where this decrease is due to softer radiation fields. Pierini et al. (1999) also see a decrease in $L_{[CII]}/L_{FIR}$ with decreasing star formation in quiescent galaxies. In early-type galaxies with little or no star-formation, $L_{[CII]}$ is lower because UV photons are needed to heat the gas by photoelectrons, whereas both optical and UV photons can heat the dust. This scenario is corroborated by high ratios of $L_{CO}/L_{[CII]}$ in some early-type galaxies (Malhotra et al 2000). At the other morphological extreme, irregular galaxies show high $L_{[OIII]}/L_{FIR}$ (Figure 6) and much of the [C II] seen in these galaxies may be originating in the ionized regions (Hunter et al. 2001). Apart from these effects, we do not see much dependence on galaxy morphology.

Because carbon has an ionization potential lower than hydrogen, [C II] emission can arise in both ionized and predominantly neutral media. The observed ratio $L_{[OI]}/L_{[CII]}$ is lower than the ratio in PDR models, suggesting a possible contribution of [C II] emission from ionized gas. In addition, the ratio of [C II] and [NII] fluxes trace each other reasonably well in the spatially resolved data in the Milky Way (Bennett et al. 1994). These two facts suggest that a fair fraction of [C II] arises in ionized regions. It is also significant that $L_{[OI]}/L_{[CII]}$ shows a remarkably tight correlation with $F_\nu(60\ \mu m)/F_\nu(100\ \mu m)$ which is as expected from PDR models, suggesting that a significant fraction of [C II] arises from PDRs. Thus the PDRs and diffuse ionized gas are associated with each other.

We estimate a scaling between [NII](122 μm) and [C II] (158 μm) from diffuse and dense ionized gas and use that scaling to estimate the [C II] luminosity from neutral regions $L_{[CII]_c}$. The main uncertainty in this calculation comes from the relative abundances of C and N. Additional uncertainty is contributed by the unconstrained fraction of the [C II] and [NII] emission arising from dense vs. diffuse ionized medium, since the scaling of $L_{[CII]}/L_{[NII]}$

is different for the two.

By comparing the observed ratios of the [O I](63μm) and the [CII]$_c$ lines from PDRs and the ratio of line to the total FIR continuum from dust with a grid of PDR models (Kaufman et al. 1999), we derive the average G_0 to be in the range $10^2 - 10^{4.5}$, and gas densities n in the range $10^2 - 10^{4.5}\,\mathrm{cm}^{-3}$ for this sample of galaxies. The FUV flux G_0 and gas densities n correlate with each other and G_0 increases roughly proportional to $n^{1.4}$ over about two orders of magnitude. We also derive G_0 and n from the observed values of $L_{[OI]}/L_{FIR}$ vs $F_\nu(60\ \mu\mathrm{m})/F_\nu(100\ \mu\mathrm{m})$. Averaged over the sample there is no systematic difference between G_0 and n derived by the two methods. Half the galaxies show better than a factor of two agreement in G_0 and n derived from the two methods.

The correlation between G_0 and n is explained by assuming that a significant portion of the PDR emission comes from PDRs surrounding expanding H II regions. The range in values of G_0 and n derived for this sample suggests that the GMCs in which OB stars are born have different average properties from galaxy to galaxy. We suggest that the galaxies with higher G_0 and n have more massive GMCs.

We thank the anonymous referee for valuable comments that improved this paper. This work was supported by ISO data analysis funding from NASA, and carried out at IPAC and the JPL of the California Institute of Technology. SM's research funding is provided by NASA through Hubble Fellowship grant # HF-01111.01-98A from the Space Telescope Science Institute, which is operated by the Association of Universities for Research in Astronomy, Inc., under NASA contract NAS5-26555. ISO is an ESA project with instruments funded by ESA Member States (especially the PI countries: France, Germany, the Netherlands and the United Kingdom), and with the participation of ISAS and NASA. This research has made use of the NASA/IPAC Extragalactic Database (NED) which is operated by the JPL, California Institute of Technology, under contract with the NASA.

A. Sample selection

This sample was constructed to study star-formation and the ISM in normal galaxies. Here normal galaxies are deined to have the energy production in the galaxy come from star-formation and not active nuclei.

The distant galaxies were selected to span a range of galaxy properties (Dale et al. 2001):

(1) Morphology: The morphology of the galaxies in this sample ranges from Irr through E (Table 5). The galaxies are uniformly distributed across the range of morphological types (see Dale et al. 2000).
(2) Far-infrared luminosity: The FIR luminosity of galaxies in this sample span the range $\mathrm{Log}(L_{FIR}/\ L_{\odot})$=7.7-11.2. Since this is a study of normal galaxies, we avoided ultra-luminous galaxies which might harbor hidden AGNs.
(3) $F_\nu(60\ \mu\mathrm{m})/F_\nu(100\ \mu\mathrm{m})$: The ratio of FIR fluxes in the IRAS filters at 60 and 100 μm indicates the average dust temperature in the galaxies. The galaxies in the sample cover the range $F_\nu(60\ \mu\mathrm{m})/F_\nu(100\ \mu\mathrm{m}) = 0.3 - 1.37$.
(4) L_{FIR}/L_B: The FIR to B-band flux ratio is a measure of star-formation activity and of dust optical depth. For low values of L_{FIR}/L_B one can approximate L_{FIR} as surrogate of extincted UV and hence current star-formation, while L_B represents relatively old stars. High values of L_{FIR}/L_B indicate high star-formation rates as well as high optical depth in dust.

Care was taken during sample selection to sample the parameter space in these four parameters: morphology, IR luminosity, $F_\nu(60\ \mu\mathrm{m})/F_\nu(100\ \mu\mathrm{m})$ and L_{FIR}/L_B, as much as possible. For a randomly selected sample, the quantities IR luminosity, $F_\nu(60\ \mu\mathrm{m})/F_\nu(100\ \mu\mathrm{m})$ and L_{FIR}/L_B, correlate with each other. We have tried to reduce these correlations by picking galaxies that sample the parameter space as uniformly as possible. Still, correlations between IR luminosity, $F_\nu(60\ \mu\mathrm{m})/F_\nu(100\ \mu\mathrm{m})$ and L_{FIR}/L_B, remain and are illustrated in Figure 14.

B. Measured Line fluxes

C. Physical quantities derived from comparison with models

REFERENCES

Bakes, E, Tielens, A 1994, ApJ, 427, 822

Bennett, C.L., Fixsen, D.J., Hinshaw, G. et al. 1994, 434, 587.

Boreiko, R.T., Betz, A.L., 1997, ApJS, 111, 409.

Blum, Robert D. & Pradhan, Anil K. 1992, ApJS, 80, 425

Brown, B.W.M., Hollander, M., & Korwar, R.M. 1974 in Reliability and Biometry ed. F. Proschan and R.J. Serfling (Philadelphia: SIAM) p327.

Clegg et al. 1996, A&A, 315,L38. 73, 359.

Cox, P. et al. 1999, in Universe as seen by ISO, ed. Cox, P., Kessler, M.

Crawford, M.K., Genzel, R., Townes, C., Watson. D.W. 1985, ApJ,291 , 755.

Dale et al. 2000, AJ, 120, 583

Dale et al. 2001, ApJ, 549, 215

Dalgarno, A., McCray, R, 1972, ARAA, 10, 375.

Esteban, C., Peimbert, M., Torres-Peimbert, S. & Escalante, V. 19 98, MNRAS, 295, 401

Ferguson, A M. N., Wyse, R F. G. & Gallagher, J. S. 1996, AJ, 11 2, 2567

Fischer, J. et al. 1999, in Universe as seen by ISO, ed. Cox, P., Kessler, M.

Froese-Fischer, C., & Saha, H.P. 1985, Phys. Scr., 32, 181 & S aha 1985

Froese-Fischer, C. 1983, J.Phys.B., 16, 157

Gavazzi, G. Boselli, A. & Kennicutt, R 1991, AJ, 101, 1207

Genzel, R. 1991, in The Galactic Interstellar Medium, ed: Burton, Elmegreen and Genzel, Springer Verlag.

Genzel, R., et al. 1998, ApJ, 498, 579

Gerin, M & Phillips, T. G. 1998, ApJ, 509, L17

Habing, H. 1968, Bull. Astr. Inst. Netherlands, 19, 421.

Heiles, C, 1994, ApJ, 436, 720.

Heckman, T. M., Armus, L. & Miley, G. K. 1990, ApJS, 74, 833

Helou, G., Khan, I., Malek, L, Boehmer, L. 1988, ApJS, 68, 151.

Helou, G., 1999, in Universe as seen by ISO, ed. Cox, P., Kessler, M.

Helou, G., Malhotra, S., Beichman, C., Dinerstein, H. et al. 1996, A&A, 315, 157.

Helou, G., Malhotra, S., Hollenbach, D.H., Dale, D.A., Contursi, A., 2001, ApJ, 548, L73.

Hollenbach, D. and McKee, C. F. 1989, ApJ, 3 42, 306

Hollenbach, David J., Takahashi, Takamasa & Tielens, A. G. G. M. 1991, ApJ, 377, 192

Hollenbach, D.J., Tielens, A.G.G.M. 1999, Rev. Mod. Phys., 7 1, 173

Hunter et al. 2000, in prep.

Isobe, T., Feigelson, E. D. & Nelson, P. I. 1986, ApJ, 306, 490

Jaquet, R., Staemmler, V., Smith, M. D. and Flower, D. R. 1992, Journalof Physics B Atomic Molecular Physics, 25, 285.

Kaufman, M., Wolfire, M.G., Hollenbach, D., Luhman, M 1999, ApJ, in press.

Keene, J., et al. 1999, in Universe as seen by ISO, ed. Cox, P., Kessler, M.

Kessler, et al., 1996, A&A, 315, L27. B.T. 1995, ApJS, 98, 129.

Kraemer, Jackson & Lane, A. P. 1996, B.A.A.S., 189, 21.02

Kennicutt, R C., Jr., Bresolin, F, B, Dominik J., Bothun, G D. & Thompson, I B. 1995, AJ, 109, 594

Kennicutt, R C., Jr. 1998, ApJ, 498, 541

Launay, J. M. and Roueff, E. 1977, A&A, 56, 289

Lennon, D.J. & Burke, V.M. 1994, A&AS, 103, 273 5, 117.

Luhman, M.L., et al. 1998, ApJ, 504, L11.

Madden, S.C., Geis, N., Genzel, R., Hermann, F., Jackson, J., Pogl itsch, A., Stacey, G.J., Townes, C.H. 1993, ApJ, 407, 579.

McKee, C. F. & Williams, J. P. 1997, ApJ, 476, 144

Malhotra, S. et al. 1997, ApJ, 491, L27

Malhotra, S. et al. 1999, in Universe as seen by ISO, ed: Cox, P., Kessler, M.

Malhotra, S. et al. 2000, ApJ, 543, 634

Meurer, G. R., Heckman, T. M., Lehnert, M. D., Leitherer, C. & Lowenthal, J. 1997, AJ, 114, 54

Meyer, D. M., Cardelli, J. A. & Sofia, U. J. 1997, ApJ, 490, L1 03

Nakagawa, T., Doi, Y., Yui, Y.Y., Okuda, H., Mochizuki, K., Shibai , H., Nishimura, T., Low, F.J., 1995, ApJ, 455, L35.

Petuchowski, S. J. & Bennett, C. L. 1993, ApJ, 405, 591

Pierini et a., 1999, MNRAS, 303, L29

Poglitsch, A., Herrmann, F., Genzel, R., Madden, S.C, Nikola, T., Timmermann, R., Geis, N., Stacey, G., 1996, ApJ, 462, L43. MNRAS, 218, 19P.

Rubin, R.H., Simpson, J.P., Haas, M.R., Erickson, E.F., 1991, ApJ, 374, 564.

Rubin, R H., Dufour, R J. & Walter, D K. 1993, ApJ, 413, 242

Rubin, R.H., Simpson, J.P., Lord, S.D., Colgan, S.W.J., Erickson, E.F., Haas, M.R. 1994, ApJ, 420, 772.

Russell, R.W., Melnick, G., Gull, G.E., Harwit, M. 1980, ApJ, 240, L99.

Sanders, D.B., Scoville, N.Z., Soifer, B.T., 1991, ApJ, 370, 158.

Schmidt, M. 1959, ApJ, 129, 243

Sofia, U. J., Cardelli, J. A., Guerin, K. P. & Meyer, D. M. 1997, ApJ, 482, L105

Sofia, U J., Cardelli, J A., Guerin, K. P. & Meyer, D. M. 1997, ApJ, 482, L105

Spitzer, L. 1978, Physical Processes in the Interstellar medium, J ohn Wiley & Sons.

Stacey, G. J., Smyers, S. D., Kurtz, N. T. & H arwit, M. 1983, ApJ, 265, L7

Stacey, G.J., Viscuso, P.J., Fuller, C.E., Kurtz, N. T.; 1985, ApJ , 289, 803.

Stacey, G. J., Jaffe, D. T., Geis, N., Grenzel, R., Harris, A. I., Poglitsch, A., Stutzki, J. & Townes, C. H. 1993, ApJ, 404, 219

Stacey, G.J., Geis, N., Genzel, R., Lugten, J.B., Poglitsch, A., Sternberg, A., Townes, C.H. 1991, ApJ, 373, 423.

Sternberg, A., Dalgarno, A. 1989, ApJ, 338, 197

Sturm, E., et al. 1996, A&A, 315, L133

Swinyard, B. M., et al. 1998, Proc. SPIE, 3354, 888

Tielens, A., Hollenbach, D., 1985, ApJ, 291, 722 (TH85). B.T. 1995, ApJS, 98, 171.

Walterbos, R A. M. & Braun, R 1994, ApJ, 431, 156

Weingartner & Draine 1999, astro-ph 9907251

Wolfire, M., Tielens, A., Hollenbach, D., 1990, ApJ, 358, 116 (WTH 90).

Wright, E.L., Mather, J.C., Bennett, C.L., et al. 1991, 381, 200.

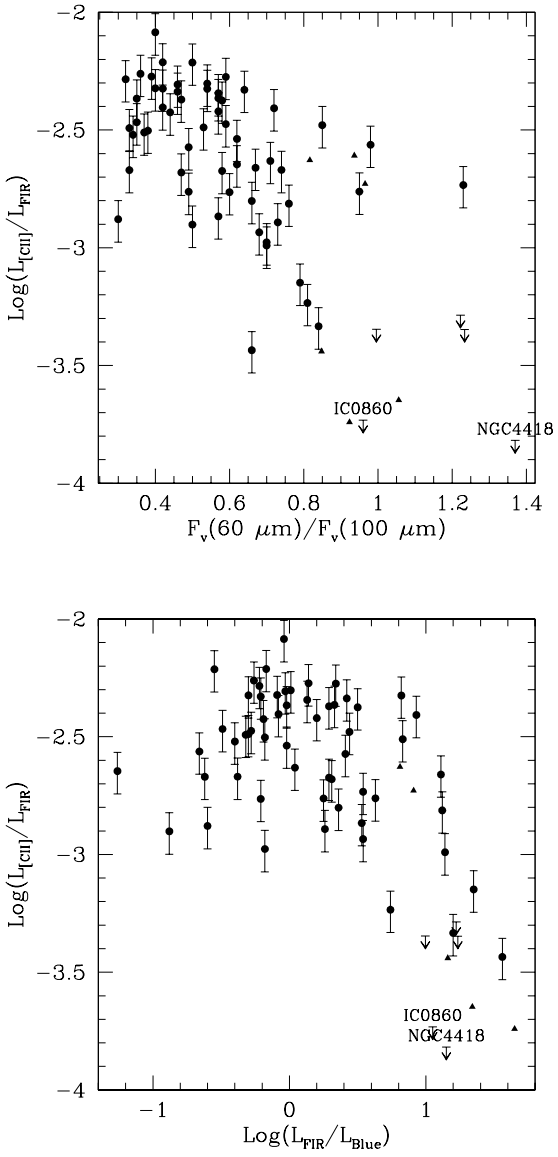

Fig. 1.— (a) The ratio of [C II] to far-infrared continuum, $L_{[CII]}/L_{FIR}$, is plotted against the ratio of flux in the IRAS 60μm and 100μm bands, $F_\nu(60\ \mu m)/F_\nu(100\ \mu m)$. Filled circles are normal galaxies from the ISO-KP sample and triangles are luminous and ultraluminous galaxies from the sample of Luhman et al. (1998). The line fluxes are uncertain by about 20%. There is a trend for galaxies with higher $F_\nu(60\ \mu m)/F_\nu(100\ \mu m)$ (indicating warmer dust) to have lower $L_{[CII]}/L_{FIR}$, for normal as well as ULIRGs. Two normal galaxies in a sample of 60 have no detected [C II], and they are identified with labels and shown as upper limit symbols in the figure; other upper limits come from Luhman et al. (1998). Rank correlation tests show that $L_{[CII]}/L_{FIR}$ and $F_\nu(60\ \mu m)/F_\nu(100\ \mu m)$ are correlated at the 4.4σ level. (b) $L_{[CII]}/L_{FIR}$ shows a similar but weaker trend (2.8σ significant) with the ratio L_{FIR}/L_B, which is an indicator of star formation activity and optical depth in dust. Galaxies with higher L_{FIR}/L_B (more active star formation) have lower $L_{[CII]}/L_{FIR}$. The decrease in $L_{[CII]}/L_{FIR}$ with L_{FIR}/L_B is not continuous but sets in for galaxies with $L_{FIR}/L_B > 0.8$.

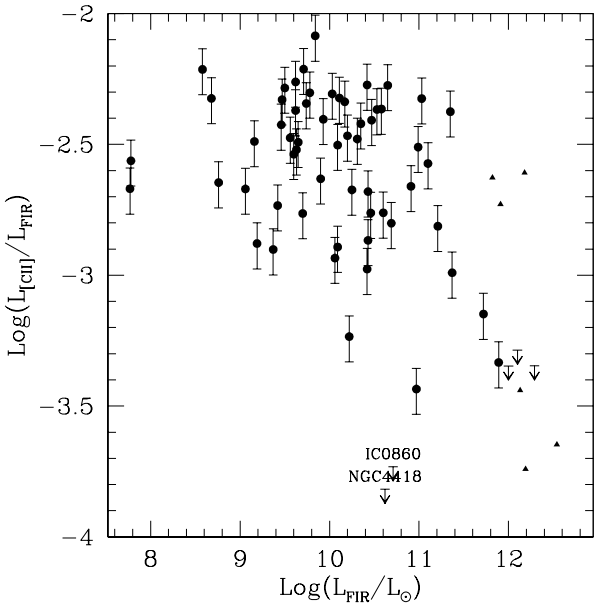

Fig. 2.— The ratio $L_{[CII]}/L_{FIR}$ plotted against the far-infrared luminosity of galaxies, L_{FIR}. Filled circles represent normal galaxies from the ISO Key Project sample and triangles denote luminous and ultraluminous galaxies from the sample of Luhman et al. (1998). There is a trend for galaxies with higher luminosity to have lower $L_{[CII]}/L_{FIR}$. Two normal galaxies in a sample of 60 and three ULIRGs have no detected [C II]; they are identified and shown as upper limit symbols in the figure. The correlation between luminosity and $L_{[CII]}/L_{FIR}$ is weakened by having the [C II] deficient normal galaxies in the middle of the luminosity range.

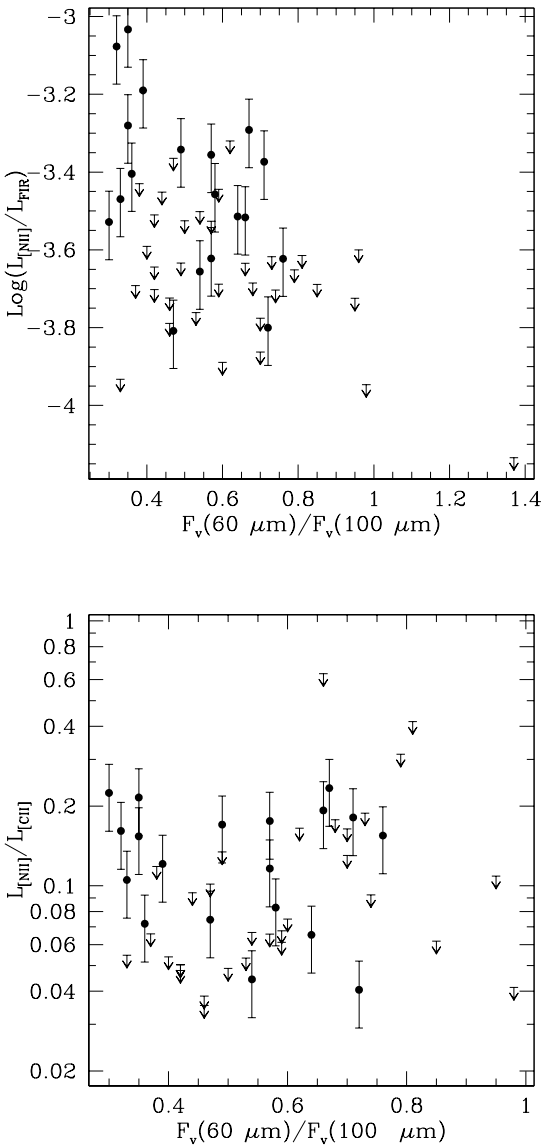

Fig. 3.— (a) The [NII] (122μm) line shows a fairly similar behavior to the [C II] line, i.e. $L_{[NII]}/L_{FIR}$ decreases at high $F_\nu(60\ \mu m)/F_\nu(100\ \mu m)$. This anticorrelation is 2.5σ significant. If true, this suggests either that (much of) [C II] and [NII] arise from H II regions, or that the PDRs which produce [C II] are associated with or surround the ionized gas which produces [NII]. The upper limits shown in this figure are 3σ upper limits. (b) This is further illustrated by the lack of any observed trends in $L_{[NII]}/L_{[CII]}$ vs $F_\nu(60\ \mu m)/F_\nu(100\ \mu m)$. The observed $L_{[NII]}/L_{[CII]} = 9^{+6}_{-6}$.

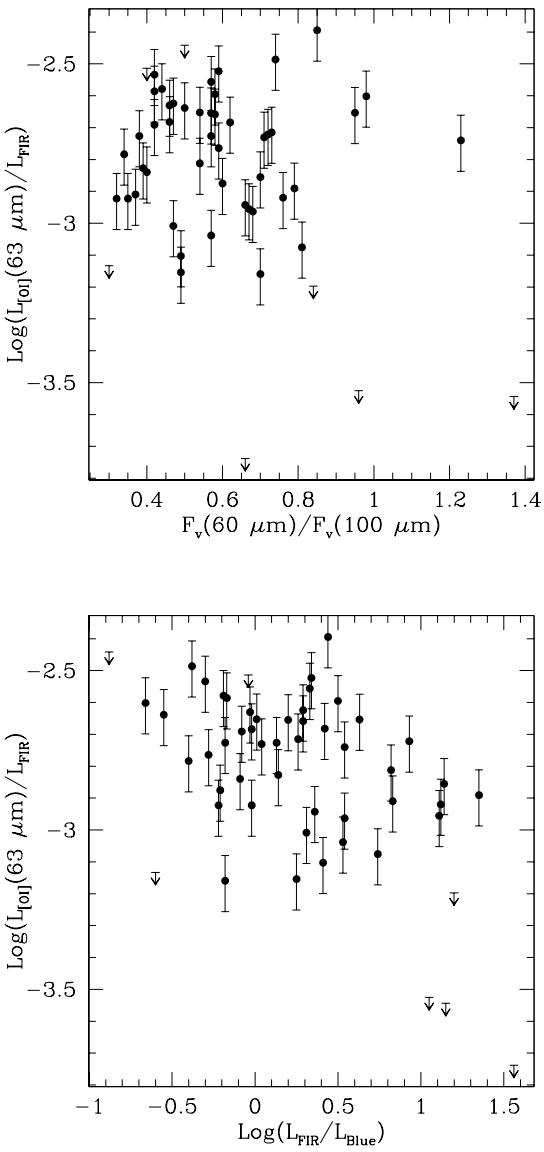

Fig. 4.— $L_{[OI]}/L_{FIR}$ shows no trends with FIR colors or FIR-to-blue ratio, except for the non-detections for galaxies with [C II] deficiency. In detected sources alone, the observed $L_{[OI]}/L_{FIR}$ ranges over a factor of six, as opposed to a factor of 60 for $L_{[CII]}/L_{FIR}$.

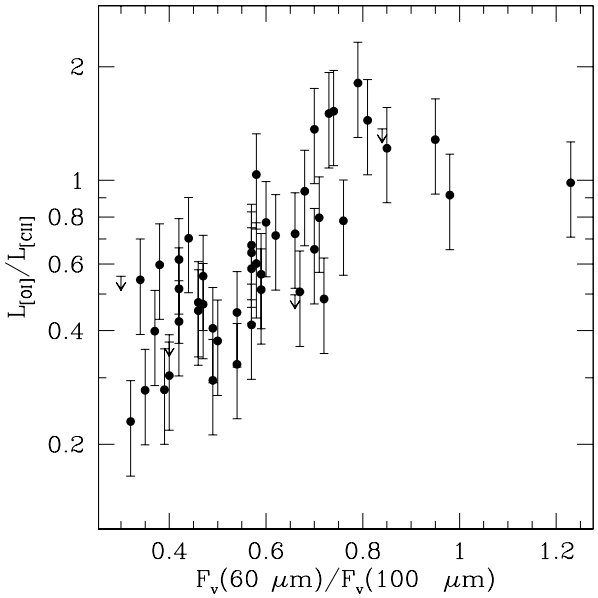

Fig. 5.— The ratio of the main cooling lines for neutral gas, $L_{[OI]}/L_{[CII]}$, shows a tight correlation with FIR colors (5.5σ significant), indicating that warm gas (which emits more [O I] (63μm) relative to [C II]) correlates with warm dust as indicated by high $F_\nu(60\ \mu m)/F_\nu(100\ \mu m)$. The observed trend is consistent with the PDR models which ascribe the increase in temperature in gas and dust to higher FUV flux G_0. [C II] dominates the cooling for galaxies with $F_\nu(60\ \mu m)/F_\nu(100\ \mu m) < 0.8$, and in galaxies with warmer dust [O I](63μm) becomes more important.

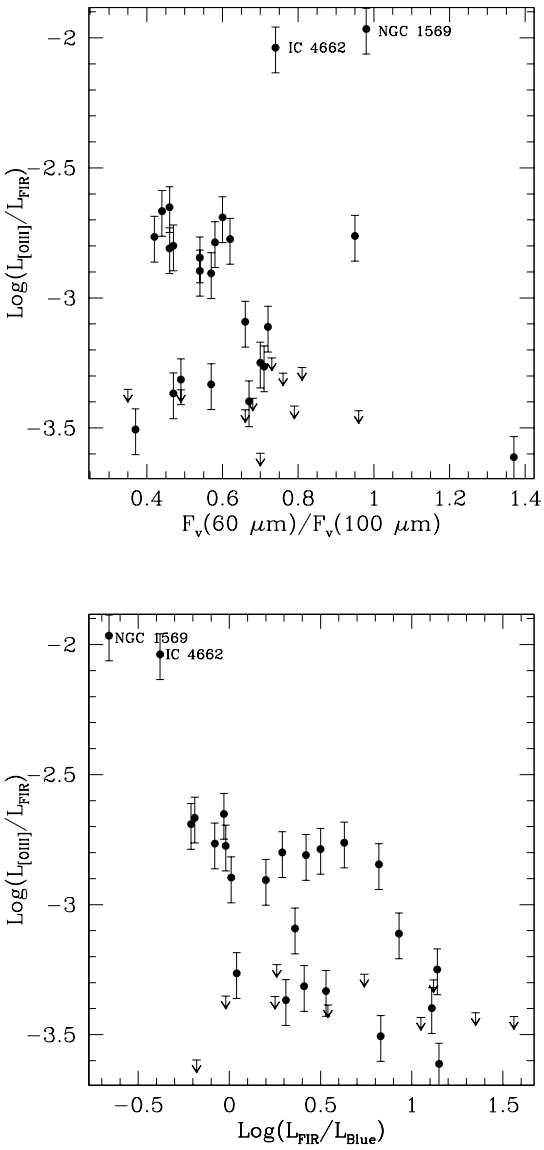

Fig. 6.— $L_{[OIII]}/L_{FIR}$ does not vary with FIR colors (the correlation between $L_{[OIII]}/L_{FIR}$ and $F_\nu(60\ \mu m)/F_\nu(100\ \mu m)$ is only 1.2 σ significant). $L_{[OIII]}/L_{FIR}$ shows an anticorrelation with L_{FIR}/L_B (3.8 σ significant), which is largely contributed by the two irregular galaxies, NGC 1569 and IC 4662, which have the lowest L_{FIR}/L_B and have very high $L_{[OIII]}/L_{FIR}$. In fact, [O III] is the strongest far-infrared line in these galaxies.

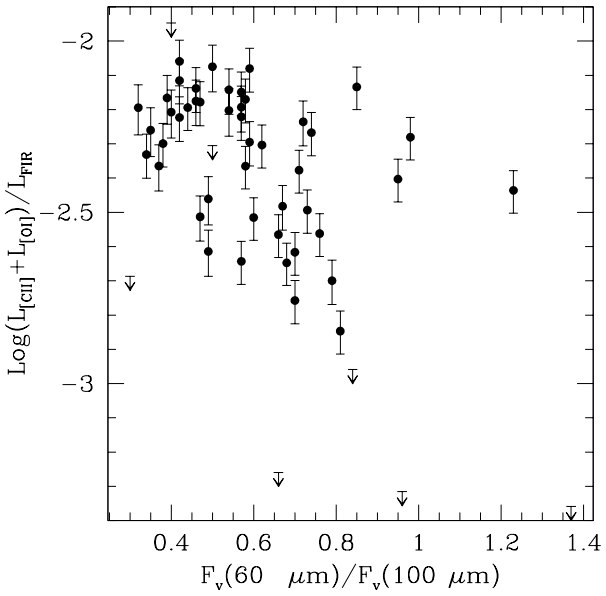

Fig. 7.— Heating efficiency $(L_{[CII]}+L_{[OI]})/L_{FIR}$ vs grain temperature $F_\nu(60\ \mu m)/F_\nu(100\ \mu m)$. A decline in the total cooling in these lines with respect to FIR is seen in galaxies with warmer dust temperatures as indicated by $F_\nu(60\ \mu m)/F_\nu(100\ \mu m)$. This is expected as grains become more positively charged in regimes of high G_0/n. The rank correlation test yields that the anticorrelation between $(L_{[CII]} + L_{[OI]})/L_{FIR}$ and $F_\nu(60\ \mu m)/F_\nu(100\ \mu m)$ is 3.3σ significant.

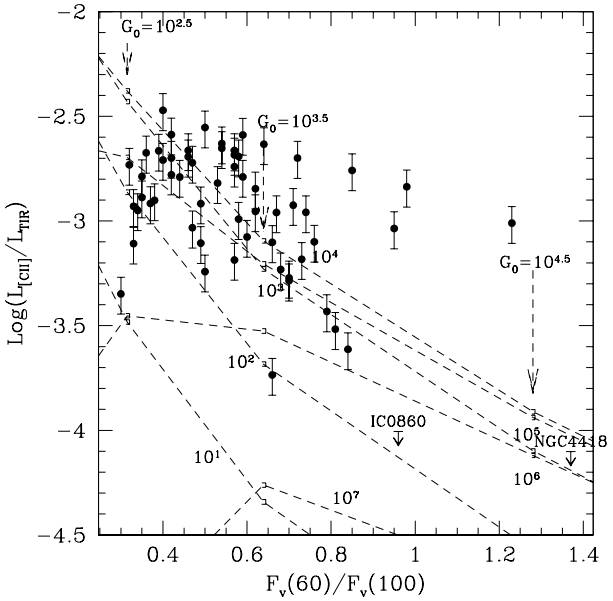

Fig. 8.— Comparison of $L_{[CII]}/L_{TIR}$ with PDR models. TIR is the total IR emission (3-1100 μm; see text). The solid dots represent the $L_{[CII]}/L_{TIR}$ values for the 60 galaxies in this sample. The curves represent $L_{[CII]}/L_{TIR}$ values for gas densities from 10^1 to $10^7\,cm^{-3}$, with notches indicated for the progression of G_0, from the PDR models of Kaufman et al. 1999. Lines of constant G_0 are vertical in this plot. The FIR colors become warmer for higher G_0. We see that the trend of decreasing $L_{[CII]}/L_{TIR}$ with $F_\nu(60\ \mu m)/F_\nu(100\ \mu m)$ is explained by the models as being due to the increase in G_0.

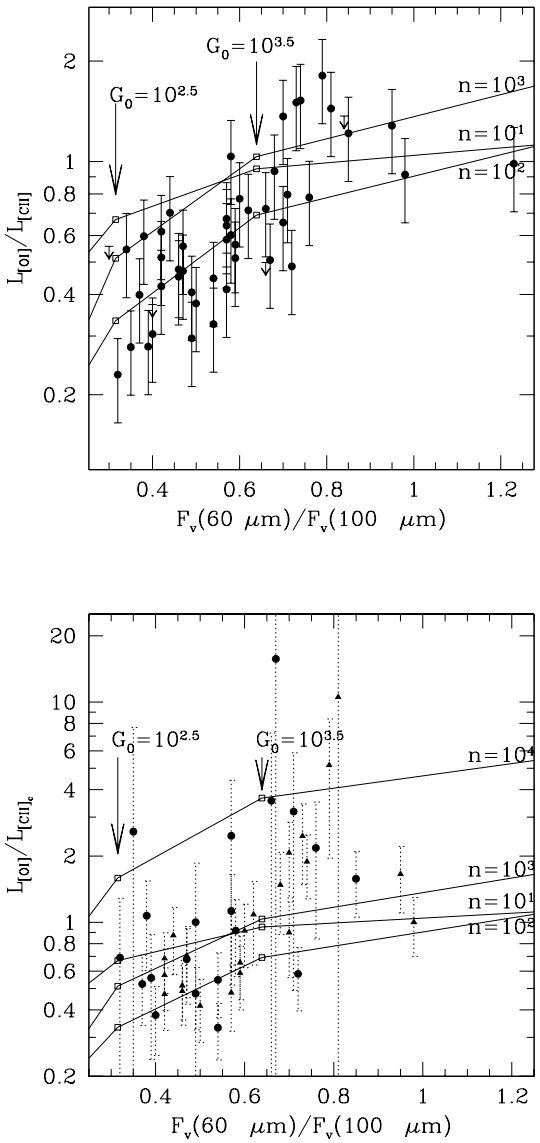

Fig. 9.— (a) The observed correlation between the ratio of the two PDR cooling lines $L_{[OI]}/L_{[CII]}$ and the dust temperature as indicated by $F_\nu(60\ \mu m)/F_\nu(100\ \mu m)$ is shown by the solid dots and upper limits. This is compared to theoretical PDR models (Kaufman et al. 1999). While the models run parallel to the trends seen, $L_{[OI]}/L_{[CII]}$ in some models is too high for about half the sample. (b) The same comparison is made, except we attempt to subtract the contribution to [C II] luminosity from ionized gas by scaling with [NII] luminosity. The solid points are where [NII] was detected, and the triangles are where we used the 2-σ upper limits on the [NII] measurements. We see that the scatter in the correlation increases because of the uncertainties in [NII] observations and the scaling factor used to subtract the [C II] emission due to ionized gas (cf section 5.1). The correlation between $L_{[OI]}/L_{[CII]}$ and $F_\nu(60\ \mu m)/F_\nu(100\ \mu m)$ persists, and the PDR models better fit the data.

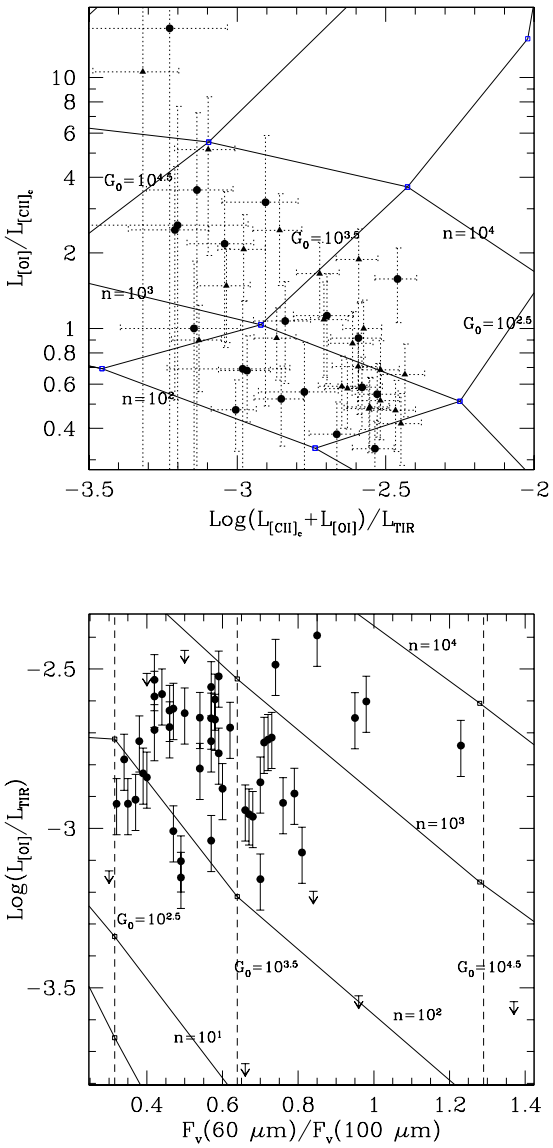

Fig. 10.— (a) The measured ratios $L_{[OI]}/L_{[CII]_c}$ and $(L_{[OI]}+L_{[CII]_c})/L_{TIR}$ (circles and triangles) are overplotted with a grid of PDR model values of the same. Solid lines are contours of constant gas density n and the dotted lines are contours of constant FUV radiation flux G_0. Two regimes of G_0 and n reproduce the observed ratios. Only one is shown here for clarity. The other regime is ruled out as it would not produce the observed [C II] and [O I] fluxes. The observed points are as in Figure 10: filled circles represent values where [C II] was corrected for the contribution from ionized gas using measured values of [NII], and triangles are where upper limits for [NII] were used. (b) The measured ratios of $L_{[OI]}/L_{TIR}$ and $F_\nu(60\ \mu m)/F_\nu(100\ \mu m)$ are plotted along with a grid of $L_{[OI]}/L_{TIR}$ and $F_\nu(60\ \mu m)/F_\nu(100\ \mu m)$ values calculated according to PDR models of Kaufman et al. (1999) and dust models of Hollenbach, Takahashi & Tielens (1991).

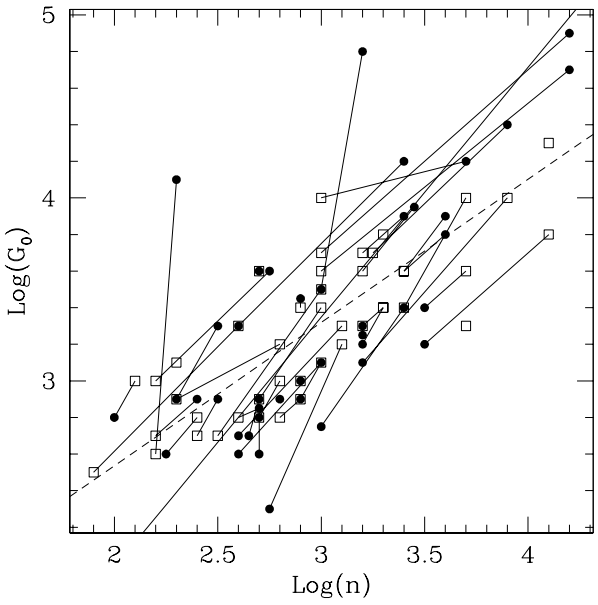

Fig. 11.— This figure shows the G_0 and n solution for galaxies based on comparison of data and PDR models shown in figure 11. The filled circles are G_0 and n values estimated from $L_{[OI]}/L_{[CII]_c}$ and $(L_{[OI]} + L_{[CII]_c})/L_{TIR}$; and the open squares are the G_0 and n values derived from $L_{[OI]}/L_{TIR}$ and $F_\nu(60\ \mu m)/F_\nu(100\ \mu m)$. The G_0 and n values derived from the two methods are connected for each source to give an estimate of the uncertainty in the parameters. A least squares fit is made to both sets of G_0 and n values assuming equal error in both axes. The best fit slopes are 1.4 and 1.3 respectively, i.e. $G_0 \propto n^\alpha$, with $\alpha = 1.3-1.4$, which is consistent with the emission coming from PDRs surrounding ionization-bounded expanding H II regions.

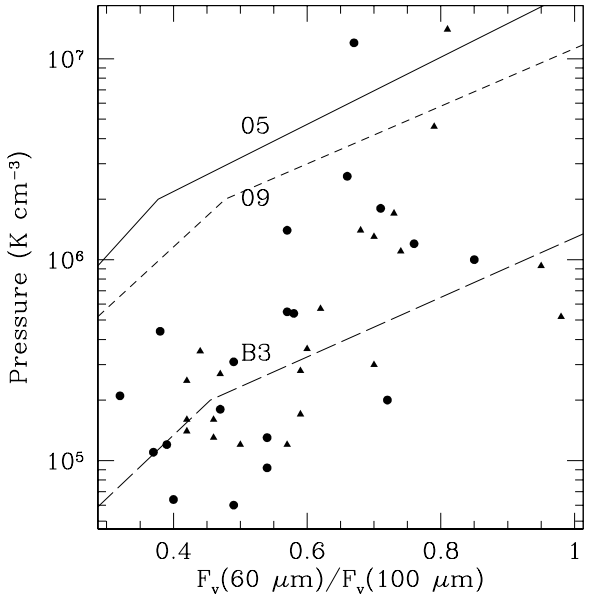

Fig. 12.— The average pressure near star forming regions in the galaxies is plotted against the FIR colors. The pressure is a product of the gas densities n and temperatures T derived from the PDR models. Both n and T increase with $F_\nu(60\ \mu m)/F_\nu(100\ \mu m)$, but the increase in n is more dramatic and is responsible for the correlation between pressure and $F_\nu(60\ \mu m)/F_\nu(100\ \mu m)$. These pressures likely do not reflect the average thermal pressure of the ISM, but do represent the pressures in PDRs surrounding H II regions associated with O and B stars. Curves are shown for the pressure in PDRs surrounding H II regions formed by stars of different spectral types (see text).

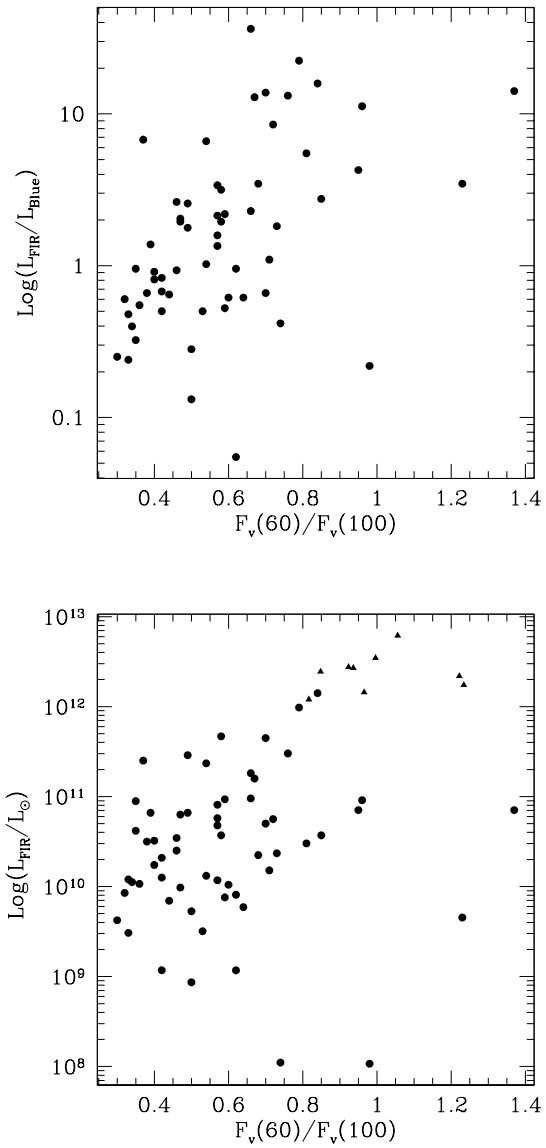

Fig. 13.— These two figures show how the galaxies discussed in this paper span the parameter space along the parameters $F_\nu(60\ \mu m)/F_\nu(100\ \mu m)$, L_{FIR}/L_B and infrared luminosity. In figure 13(a), a correlation between $F_\nu(60\ \mu m)/F_\nu(100\ \mu m)$ and L_{FIR}/L_B is seen. This correlation is 4.5 σ significant. Figure 13(b) also shows in triangles the luminous and ultraluminous galaxies from the sample of Luhman et al. (1998). The correlation between $F_\nu(60\ \mu m)/F_\nu(100\ \mu m)$ and L_{FIR} is 4.1σ significant.

Table 5: The sample

Galaxy	Morphology	$F_\nu(60\mu m Jy)$	$\frac{F_\nu(60\mu m)}{F_\nu(100\mu m)}$	$\frac{L_{FIR}}{L_B}$	FIR $(10^{-14} W/m^2)$
NGC 0278	SAB(rs)b	25.05	0.54	0.01	139.9
NGC 520	Irr	31.1	0.66	0.36	160.5
NGC 0693	I0: sp	6.73	0.57	0.13	36.75
NGC 0695	IB?(s)m: pec	7.87	0.58	0.5	42.68
UGC 01449	SBm; pec:	4.96	0.59	0.34	26.72
MCG-03-06-01	SB0 pec:	4.41	1.23	0.54	18.85
NGC0986	(R´_1)SB(rs)b	25.14	0.49	0.25	146.4
NGC1022	(R)́SB(s)a	19.83	0.73	0.26	98.69
NGC1052	E4;Liner;Sy2	0.93	0.62	-1.26	4.913
UGC02238	Pec	8.4	0.54	0.82	46.91
NGC1155	(R)́SAB(s)0o: pec	2.89	0.58	0.29	15.67
NGC1156	IB(s)m	5.24	0.5	-0.55	30.24
NGC1222	S0-pec:	13.07	0.85	0.44	61.86
UGC02519	SAB?(s:)cd III:	2.98	0.4	-0.04	19.07
NGC1266	(R)́SB(rs)0 pec;Liner	13.32	0.81	0.74	64.02
NGC1317	(R)́SAB(rl)0/a	3.52	0.34	-0.4	24.49
NGC1326	(R-1)SB(rl)0/a;Liner	8.17	0.59	-0.28	44.01
NGC1385	SB(s)cd	17.3	0.46	-0.03	103.6
UGC02855	SB(s)cd II-III	42.39	0.47	0.31	251.4
NGC1482	SA0+;pec;sp	33.45	0.72	0.93	167.3
NGC1546	SA?a pec	7.21	0.32	-0.22	51.83
NGC1569	IBm;Sy1	54.25	0.98	-0.66	246.1
NGC2388	SA(s)b: pec	17.01	0.67	1.11	87.29
ESO317-G023	(R-́1)SB(rs)a	13.5	0.57	0.53	73.73
IRASF10565+2	Pec	12.08	0.79	1.35	58.54
NGC3583	SB(s)b	7.08	0.38	-0.18	46.49
NGC3620	(R´_1)SB(s)ab	46.8	0.7	-0.18	236.4
NGC3683	SB(s)c?	13.61	0.46	0.42	81.52
NGC3705	SAB(r)ab	3.72	0.33	-0.62	26.3
NGC3885	SAB(r:)0/a:	11.66	0.71	0.04	58.6
NGC3949	SA(s)bc:	11.28	0.44	-0.19	68.97
NGC4027	SB(s)dm	11.61	0.42	-0.08	72.57
NGC4102	SAB(s)b?;Liner	48.1	0.68	0.54	245.5
NGC4194	IBm;pec	23.81	0.95	0.63	109
NGC4418	(R)́SAB(s)a	43.89	1.37	1.15	183
NGC4490	SB(s)d;pec	45.9	0.6	-0.21	245.6
NGC4519	SB(rs)d	3.74	0.53	-0.3	21.05
NGC4691	(R)SB(s)0/a;pec	14.43	0.62	-0.02	76.23
NGC4713	SAB(rs)d	4.6	0.42	-0.3	28.75
IC3908	SB(s)d?	8.09	0.47	0.29	47.99
IC0860	SB(s)a:	17.93	0.96	1.05	81.82
IC0883	Pec	17.01	0.7	1.14	85.91
NGC5433	SAB(s)c:	6.62	0.57	0.33	36.15
NGC5713	SAB(rs)bc pec	21.89	0.57	0.2	119.5
NGC5786	(R´_2)SAB(s)bc	5.26	0.35	-0.49	36.04
NGC5866	S0_3;HII/Liner	5.21	0.3	-0.6	38.82
CGCG1510.8+0	SB?(s?)0/a pec	20.84	0.66	1.56	107.5
NGC5962	SA(r)C	8.89	0.4	-0.09	56.9
IC4595	SB?c sp II:	7.05	0.39	0.14	45.7
NGC6286	SB(s)0+ pec?	8.22	0.37	0.83	54.71
IC4662	IBm	8.81	0.74	-0.38	43.64
NGC6753	(R)SA(r)b	9.77	0.35	-0.02	66.93
NGC6821	SB(s)d:	3.63	0.64	-0.21	18.95
NGC6958	E+	1	0.5	-0.88	5.771
NGC7218	SB(r)c	4.67	0.42	-0.17	29.19
NGC7418	SAB(rs)cd	5.38	0.33	-0.32	38.03
IC5325	SAB(rs)bc	5.15	0.36	-0.26	34.77
IRASF23365+3	S?Ba? pec or Pec	7.44	0.84	1.2	35.35
NGC7771	SB(s)a	19.67	0.49	0.41	114.5
MRK0331	SA(s)a: pec	18.04	0.76	1.12	88.55

Table 6: Line fluxes for the distant sample (in units of $10^{-14}W/m^2$)

Galaxy	[CII](158μm)	[OI](145μm)	[NII](122μm)	[OIII](88μm)	[OI](63 μm)	[NIII] (57μm)	[OIII] (52μm)
NGC0278	0.697	< 0.014	0.031	0.178	0.312	< 0.093	< 0.102
NGC520	0.254	0.025	0.049	0.13	0.184	< 0.162	< 0.205
NGC0693	0.167	-	< 0.011	-	0.07	-	-
NGC0695	0.181	-	0.015	0.07	0.109	-	-
UGC01449	0.143	-	<0.01	-	0.081	-	-
MCG-03-06-01	0.035	-	-	-	0.035	-	-
NGC0986	0.254	< 0.027	< 0.034	< 0.065	0.103	< 0.135	< 0.068
NGC1022	0.127	-	< 0.024	< 0.058	0.191	-	-
NGC1052	0.012	-	-	-	-	-	-
UGC02238	0.222	-	< 0.015	0.068	0.073	-	-
NGC1155	0.034	-	-	-	0.035	-	-
NGC1156	0.186	-	<0.01	-	0.07	-	-
NGC1222	0.206	-	< 0.013	-	0.25	-	-
UGC02519	0.157	-	-	-	< 0.059	-	-
NGC1266	0.038	-	< 0.016	< 0.035	0.054	-	-
NGC1317	0.074	-	-	-	0.041	-	-
NGC1326	0.148	-	<0.01	-	0.076	-	-
NGC1385	0.511	-	<0.02	0.232	0.243	< 0.071	-
UGC02855	0.525	< 0.033	0.04	0.108	0.247	< 0.164	< 0.198
NGC1482	0.655	< 0.034	0.027	0.13	0.318	0.055	< 0.094
NGC1546	0.27	-	0.044	-	0.062	-	-
NGC1569	0.674	< 0.014	< 0.028	2.663	0.616	< 0.141	1.722
NGC2388	0.191	-	0.045	0.035	0.097	< 0.081	-
ESO317-G023	0.101	-	0.018	0.035	0.068	< 0.071	-
IRASF10565+2	0.042	-	< 0.014	< 0.023	0.076	-	-
NGC3583	0.147	-	< 0.018	-	0.088	-	-
NGC3620	0.25	0.029	< 0.033	<0.06	0.164	< 0.158	< 0.166
NGC3683	0.376	-	< 0.014	0.127	0.17	< 0.055	-
NGC3705	0.057	-	< 0.004	-	-	-	-
NGC3885	0.137	-	0.025	0.032	0.11	-	-
NGC3949	0.26	-	< 0.025	0.149	0.183	-	-
NGC4027	0.287	-	< 0.015	0.125	0.148	0.062	-
NGC4102	0.286	0.022	< 0.051	< 0.101	0.268	< 0.232	< 0.147
NGC4194	0.189	-	< 0.021	0.189	0.243	0.062	-
NGC4418	< 0.028	<0.02	< 0.014	0.045	< 0.053	< 0.214	< 0.213
NGC4490	0.423	0.011	< 0.032	0.502	0.328	< 0.229	0.403
NGC4519	0.069	-	< 0.004	-	-	-	-
NGC4691	0.222	-	< 0.037	0.129	0.158	< 0.103	-
NGC4713	0.137	-	< 0.007	-	0.085	-	-
IC3908	0.205	-	< 0.021	0.077	0.115	-	-
IC0860	< 0.016	-	< 0.021	< 0.031	< 0.025	< 0.346	-
IC0883	0.088	-	< 0.015	0.049	0.12	-	-
NGC5433	0.157	-	-	-	0.101	-	-
NGC5713	0.454	< 0.009	0.053	0.149	0.265	< 0.024	0.143
NGC5786	0.123	-	0.019	-	-	-	-
NGC5866	0.052	-	0.012	-	< 0.029	-	-
CGCG1510.8+0	0.04	-	< 0.025	<0.04	<0.02	< 0.059	-
NGC5962	0.271	-	< 0.015	-	0.083	-	-
IC4595	0.244	-	0.03	-	0.069	-	-
NGC6286	0.169	-	< 0.012	0.018	0.068	-	-
IC4662	0.094	-	< 0.009	0.401	0.143	-	-
NGC6753	0.288	-	0.063	<0.03	0.081	-	-
NGC6821	0.089	-	0.006	-	-	-	-
NGC6958	0.008	-	-	-	< 0.021	-	-
NGC7218	0.18	-	<0.01	-	0.076	-	-
NGC7418	0.123	-	0.013	-	-	-	-
IC5325	0.191	-	0.014	-	-	-	-
IRASF23365+3	0.017	-	-	-	< 0.023	-	-
NGC7771	0.307	-	0.053	0.056	0.091	< 0.029	-
MRK0331	0.137	-	0.022	< 0.046	0.107	-	-

Table 7: Average physical parameters derived by comparing FIR line fluxes with PDR models

Galaxy	Log(G_0) (from $L_{[OI]}/L_{FIR}$)	Log(n) cm^{-3} $L_{[OI]}/L_{FIR}$)	Log(G_0) (from $L_{[OI]}/L_{[CII]_c}$	Log(n) cm^{-3} and $(L_{[OI]} + L_{[CII]_c})/L_{TIR}$)	Temperature K	Pressure Kcm^{-3}	Pressure (HII) Kcm^{-3}
NGC0278	3.2	3.1	2.3	2.75	225	1.3×10^5	
NGC520	4.0	3.0	4.2	3.7	510	2.6×10^6	
NGC0693	3.3	3.1	2.7	2.6	310	1.2×10^5	
NGC0695	3.4	3.3	3.2	3.2	340	5.4×10^5	
UGC01449	3.4	3.4	2.75	3	280	2.8×10^5	
MCG-03-06-01	4.3	4.1	...	...	550	6.9×10^6	
NGC0986	3.0	2.1	2.8	2	600	6×10^4	
NGC1022	3.6	3.4	3.8	3.6	430	1.7×10^6	
UGC02238	3.2	2.8	2.9	2.3	460	9.2×10^4	
NGC1155	3.3	3.7	...	...	350	1.7×10^6	
NGC1156	3.1	3.0	2.6	2.6	290	1.2×10^5	
NGC1222	3.8	4.1	3.2	3.5	325	1×10^6	
NGC1266	3.7	3.0	4.9	4.2	900	1.4×10^7	
NGC1317	3.1	2.3	...	...	575	1.1×10^5	
NGC1326	3.4	3.0	2.9	2.7	340	1.7×10^5	
NGC1385	3.0	2.8	2.8	2.7	310	1.6×10^5	
UGC02855	2.9	2.3	3.3	2.5	560	1.8×10^5	
NGC1482	3.6	3.4	2.9	2.8	325	2×10^5	
NGC1546	2.5	1.9	3.3	2.6	525	2.1×10^5	
NGC1569	4.0	3.9	3.1	3.2	325	5.2×10^5	2.5×10^5
NGC2388	3.6	3.0	4.7	4.2	775	1.2×10^7	
ESO317-G023	3.3	2.6	4.2	3.4	550	1.4×10^6	
IRASF10565+2	3.7	3.25	4.4	3.9	580	4.6×10^6	
NGC3583	2.7	2.5	3.5	3	440	4.4×10^5	
NGC3620	3.6	2.7	3.6	2.7	600	3×10^5	
NGC3683	2.9	2.7	2.7	2.65	300	1.3×10^5	
NGC3885	3.6	3.4	3.9	3.6	450	1.8×10^6	
NGC3949	2.9	2.9	3.1	3	340	3.5×10^5	
NGC4027	2.8	2.6	2.85	2.7	325	1.6×10^5	
NGC4102	3.5	3.0	4.8	3.2	900	1.4×10^6	
NGC4194	4.0	3.7	3.4	3.4	370	9.3×10^5	
NGC4490	3.4	2.9	3.45	2.9	450	3.6×10^5	8×10^5
NGC4691	3.4	3.3	3.3	3.2	360	5.7×10^5	
NGC4713	2.8	2.8	2.9	2.9	310	2.5×10^5	
IC3908	3.0	2.9	3	2.9	340	2.7×10^5	
IC0883	3.6	3.2	3.95	3.45	475	1.3×10^6	
NGC5433	3.8	3.3	...	...	450	8.9×10^5	
NGC5713	3.3	3.2	3.25	3.2	350	5.5×10^5	1.3×10^6
NGC5962	2.8	2.4	2.6	2.25	360	6.4×10^4	
IC4595	2.7	2.4	2.9	2.5	390	1.2×10^5	
IC4662	3.6	3.7	3.4	3.5	360	1.1×10^6	
NGC6286	2.7	2.2	2.9	2.4	425	1.1×10^5	
NGC6753	2.6	2.2	4.1	2.3	1400	2.8×10^5	
NGC7218	2.8	2.7	2.6	2.7	270	1.4×10^5	
NGC7771	3.0	2.2	3.6	2.75	560	3.1×10^5	
MRK0331	3.7	3.2	3.9	3.4	460	1.2×10^6	